EPRI

Creep as the Limiting Mechanism for Spent Fuel Dry Storage

1001207

Creep as the Limiting Mechanism for Spent Fuel Dry Storage

1001207

Technical Progress, December 2000

EPRI Project Manager

A. Machiels

EPRI • 3412 Hillview Avenue, Palo Alto, California 94304 • PO Box 10412, Palo Alto, California 94303 • USA
800.313.3774 • 650.855.2121 • askepri@epri.com • www.epri.com

DISCLAIMER OF WARRANTIES AND LIMITATION OF LIABILITIES

ORGANIZATION(S) THAT PREPARED THIS DOCUMENT

ANATECH CORP.

This is an EPRI Level 2 report. A Level 2 report is intended as an informal report of continuing research, a meeting, or a topical study. It is not a final EPRI technical report.

ORDERING INFORMATION

Requests for copies of this report should be directed to the EPRI Distribution Center, 207 Coggins Drive, P.O. Box 23205, Pleasant Hill, CA 94523, (800) 313-3774.

CITATIONS

This report was prepared by

ANATECH Corp.
5435 Oberlin Drive
San Diego, CA 92121

Principal Investigators
Y.R. Rashid
D.J. Sunderland
R.O. Montgomery

This report describes research sponsored by EPRI.

The report is a corporate document that should be cited in the literature in the following manner:

Creep as the Limiting Mechanism for Spent Fuel Dry Storage, EPRI, Palo Alto, CA: 2000. 1001207.

ABSTRACT

Cladding creep is the dominant deformation regime for spent fuel in dry storage, and the evaluation of creep related time-dependent damage is an essential component of spent fuel storage licensing. Several potential damage mechanisms have been postulated for spent fuel in dry storage, which include accelerated (tertiary) creep leading to creep rupture, delayed hydride cracking (DHC), and stress corrosion cracking (SCC). These mechanisms are examined in detail in this report with the objective of determining their effect in potentially limiting the creep capacity of spent fuel cladding in dry storage. It is shown that the spent fuel environment lacks the conditions that are necessary for SCC and DHC mechanisms to become operative in dry storage. The prevention of creep rupture of spent fuel rods, as a safety goal for long-term storage, is demonstrated using a conservative strain-based criterion. Sufficient data and analytical modeling exist to show that a strain limit of 2% can be safely used as an asymptotic limit for fuel rods normally discharged from reactors without imposing any restrictions on oxide thickness or physical conditions.

CONTENTS

ILLUSTRATIONS

1

INTRODUCTION

Current regulatory practices governing spent fuel dry storage, NUREG-1536, 1997 [1], allow a very low probability (0.5%) of cladding failure during long-term storage. Implied in this statement is the acceptance that a small percentage of the rods (up to ~25 rods in a 24-PWR-assembly cask) may fail. Implicitly, this presumes that the requisite analytical modeling capabilities exist for predicting fuel rod failure frequency. The object of analytical modeling is the determination of two inter-dependent response states: cladding creep deformations over the projected storage life, and potential loss of cladding integrity by one of several postulated damage mechanisms. Of these damage mechanisms, the following are relevant: accelerated (tertiary) creep leading to creep rupture (CR), delayed hydride cracking (DHC), and stress corrosion cracking (SCC). The conditions that govern these failure mechanisms are strongly dependent on the initial thermo-mechanical and physical states of the cladding when first placed in dry storage. These include temperature; stress; chemical composition including hydrogen concentration, distribution, and hydride morphology; fast fluence; .... Each of these conditions plays a role, to varying degrees, in determining the deformation rate and ultimately cladding failure potential. This report will examine each of these failure mechanisms as they relate to dry storage conditions, with the objective of determining which mechanism governs the deformation capabilities of spent fuel in dry storage.

The above list of failure mechanisms leaves out a fourth mechanism [2], which is the thermally activated micro-cavitation leading to failure by diffusion-controlled cavity growth (DCCG). This mechanism is thoroughly discussed elsewhere (Hayes et al., 1999 [6]; Pescatore and Cowgill, 1994 [7]) and is excluded from consideration in this report. However, a brief historical background would be appropriate at this point.

Traditional methods for the life-prediction of structural components operating in the creep regime have utilized phenomenological models that rely on creep-strain data generated as function of stress, temperature, and time. In contrast, DCCG-based methods utilize mechanistic models that rely, not on creep data for the calculation of creep-related damage in the cladding structure, but on assumed materials microstructural parameters that are not easily measurable (e.g., grain boundary diffusion coefficient [6,7].

In the eighties, NRC reviewers invoked the DCCG mechanism for determining allowable peak cladding temperatures. The DCCG model, which has the unusual property of predicting global fracture without any strain in the material, freed the regulatory review process from having to rely on the few post-irradiation thermal creep data that were available at the time. Lawrence Livermore National Laboratories' (LLNL) version of the DCCG model (Schwartz and Witt, 1987 [3]), based on earlier work by Raj and Ashby, 1975 [4], eventually became NRC's tool for

verifying that cladding temperatures remain below expected damage thresholds for normal conditions of storage.

The NRC recently dismissed LLNL's DCCG model as being "overly restrictive and relatively inflexible" and also stated that "recently developed literature does not support the use of this model for zirconium-based materials" [8]. Finally, Ref. 8 stated its continued acceptance of the Commercial Spent Fuel Management (CSFM) methodology developed by PNNL. The CSFM methodology (Chin et al., 1986 [5]) contains five fracture mechanisms, which include the cavity growth mechanism prescribed by the DCCG model. However, there are important differences, both in the models' treatments and the numerical values of the models' parameters, between LLNL's and PNNL's versions of Raj's and Ashby's original construct of creep-cavity growth mechanism. Closer examination reveals that the DCCG damage mechanism dominates the predictions in the CSFM methodology for the stress and temperature conditions of interest to dry storage. Although the NRC continues to subscribe to PNNL's CSFM methodology, whose predictions are rooted in the DCCG model, it has stated that it will accept a strain-based model for determining the maximum initial storage temperature (ISG-11, 1999 [8]).

The approach adopted in this report is a return to traditional engineering creep methods relying on strain-based models.

2

STRESS CORROSION CRACKING (SCC) MECHANISM

Background

The emergence of stress corrosion cracking (SCC) as a fuel failure mechanism dates back to the early seventies when BWR fuel ramped to high power began to experience failures. The failure mechanism was attributed to stress corrosion cracking induced by iodine, or other corrosive fission products such as cadmium-cesium, and came to be known as PCI (pellet-cladding interaction). In the two decades after PCI established itself as a power-limiting failure mechanism for LWRs in general, considerable research was undertaken at a number of institutions. An exhaustive review of the literature describing this research is outside the scope of this report, but it is relevant to give a brief outline of the state of the art as it relates to spent-fuel dry storage.

In the earliest reported studies of iodine-induced stress corrosion cracking of Zircaloy cladding (Rosenbaum, 1966 [9]; Garlick et al., 1971 [10]), the PCI phenomenon was simulated by thermally expanding a tightly fitted stainless steel mandrel inserted into a Zircaloy tube containing iodine vapor. Subsequent research, which proliferated in the seventies and eighties, used other techniques to simulate PCI conditions, including slotted rings, pressurized tubes, cracked ceramic annulus, and fracture-mechanics specimens. This research can be grouped into three major areas: (a) fundamental material behavior tests to characterize the SCC phenomenon [9-17]; (b) special effects time-to-failure tests and analytical modeling to develop fuel response prediction methods [18-23]; and (c) test-reactor power ramp integral tests to characterize in-reactor behavior [24-28] and to support the development of PCI-resistant cladding [29-31]. The cited references, which constitute only a partial list of a very large volume of work, show that the SCC phenomenon is sufficiently well characterized to allow extrapolation to spent fuel dry storage conditions. Extrapolation of the in-reactor PCI failure mechanism to spent fuel in dry storage is examined in some detail below.

PCI Mechanism

The prerequisite for PCI failures is the concomitant release of fission products to the fuel rod gap and the generation of sufficiently high PCMI (pellet-clad mechanical interaction) stresses during power ramps. Analytical modeling of the PCMI phenomenon show that the stresses needed to initiate PCI failures had to be highly focused (concentrated at pellet cracks) and rising during the power ramp to nearly 80% of the materials yield strength [20,23]. This state of high stress, which begins to undergo rapid relaxation immediately at the end of the power ramp due to fuel-pellets compressive creep, must remain above the threshold stress for the required incubation time needed to initiate SCC. Thus, the time-at-stress combined with the simultaneous availability of corrosive fission products are the primary factors that control the PCI failure mechanism.

These conditions are not duplicated in exactly the same way in dry storage, and neither are they precisely simulated in laboratory tests, as we shall see below.

Role of Chemistry

Laboratory tests conducted in iodine vapor indicate that the minimum iodine availability for stress corrosion cracking is of the order 10^{-6} g per cm^2 (Busby et al., 1975 [32]; Peehs et al., 1979 [33]). This amount of iodine is associated with a fission gas release of less than 1%, which indicates that sufficient iodine can be released during in-reactor irradiation. Equilibrium thermodynamics, however, require that any iodine isotopes that reach the cladding should do so in the form of cesium iodide. Therefore, there must be a release of elemental iodine from cesium iodide by gamma or other forms of high-energy radiation (Cubiccioti and Davies [34]), a condition that is not duplicated in spent fuel storage. Moreover, during storage, fission gas is neither generated, nor released. The fuel temperature in storage is well below the Vitanza threshold (about 1000°C for high burnup fuel) for fission gas release from the grains to the grain boundaries and then to the fuel rod free volume. This suggests that the availability of elemental iodine in the fuel-cladding gap is too small to provide sufficient iodine flux for diffusion into the cladding to initiate SCC. Also, there is no data to indicate that SCC can be induced by solid state diffusion of cesium iodide. It can be concluded, therefore, that the iodine-related chemical environment in dry storage is sub-critical, or marginal at best, to induce SCC failures. Other forms of corrosive environments are discussed next.

Iodine may not necessarily be the only corrosive fission product that can induce SCC failures (see the discussion to Tasooji et al., Ref. 35). Arguments have been made that cadmium-cesium plays a similar role to iodine in embrittling the cladding. Cox and Haddad [36] have shown that no distinction can be made fractographically between failures obtained in the laboratory in iodine vapor and those in cadmium-cesium vapor. However, the situation is quite different under dry storage conditions, as already discussed in the case of iodine. As to cadmium-bearing cesium, it is in a liquid state at room temperature, but has a high boiling point of 671°C. The major portion of cesium would have been released to the plenum during in-reactor irradiation when it was in a predominantly gaseous state, and would partially condense there because of the lower temperature. The remainder may become attached to the fuel and cladding surfaces in the relatively low-temperature gap region. The entire inventory will have condensed to a liquid form upon reactor shutdown and removal of the fuel to the spent fuel pool. The Cox and Haddad tests referenced above [36] were conducted in cesium/cadmium vapor and at much higher stresses than normally present in spent fuel rods. Syrett et al. [37] have shown that Zr-4 embrittlement by liquid cesium can be produced in the laboratory only if the cesium has low oxygen content and is contaminated with a trace of iron. Moreover, the applied stress in the Syrett et al. experiments had to exceed the yield strength of the material, unlike iodine-induced SCC where the threshold stress is lower than the yield strength.

The above observations lead to the conclusion that extrapolation of in-reactor cadmium-cesium and iodine-related environments to dry storage cannot be justified mechanistically on the basis of the available data.

Role of Stress and Time-at-Stress

SCC failure evolves in two stages: a relatively long incubation (crack-nucleation) stage and a much shorter crack-propagation stage. The stress and the strain rate play a dominant role in determining the failure time and the failure mode: the higher the stress, the shorter the time to failure; and the higher the strain rate, the more likely the failure will be by fast crack propagation in a transgranular cleavage mode. At low stresses and low strain rates, SCC failure is predominantly by the much slower process of intergranular crack growth. As we shall further see, under the very low creep-strain rates and sub-threshold stresses, typical of dry storage conditions, intergranular cracking is nearly impossible to initiate, which would preclude the second stage of transgranular crack propagation.

Laboratory tests have shown that the incubation time depends strongly on the surface conditions of the specimen. For example, smooth specimens, or specimens with scratches or shallow flaws, were found to behave like smooth specimens with relatively long incubation time, whereas fatigue-cracked specimens with deeper sharp cracks showed considerably shorter failure times. The major portion (75%) of incubation time is taken up in creating the proper conditions needed to nucleate a crack in a previously uncracked material. Thus, if the incubation time is primarily a measure of the evolution of the crack tip geometry, then once the crack initiates and the crack-tip stress intensity factor K_I reaches the SCC fracture toughness K_{ISCC}, the crack velocity increases rapidly by several orders of magnitude (Figure 2-1), and SCC failure is completed fairly quickly in a transgranular mode. This gives rise to three major conditions that have important significance to spent fuel application. First, once the assumption is made that the appropriate corrosive environment is available in the gap, a necessary, but not sufficient, condition for failure is for the cladding stress to exceed the threshold stress for SCC. Second, a stress-dependent minimum incubation time is needed to create the proper conditions for crack nucleation. Third, once a crack tip is formed, a necessary and sufficient condition for transgranular crack propagation is a stress intensity factor K_I in excess of K_{ISCC}. Because the cladding stress changes very slowly with time in a spent fuel rod, the first and third conditions govern the SCC process in dry storage, unlike the in-reactor situation where the time-at-stress is dictated by the stress relaxation rate during and after power ramps. These conditions are interdependent and must take place sequentially before SCC can occur in dry storage. The manifestation of these conditions in dry storage is discussed below.

The laboratory data reported in the above-cited literature was obtained for a variety of test conditions. These included pressurized smooth and scratched tubes, split ring samples, double cantilever samples, notched samples with and without sharp starter cracks, as received stress-relieved samples, fully re-crystallized samples, pre-oxidized and hydrided samples, unirradiated and irradiated samples, Zr-2 and Zr-4 material, etc. A survey of the SCC data shows that for relevant temperatures (above 300°C), the threshold stress for inducing failure by SCC in internally pressurized annealed Zr-2 tube samples is approximately 360 MPa and 180 MPa for unirradiated and irradiated materials, respectively. Threshold values for stress relieved Zr-4 samples are 300 MPa and 200 MPa for unirradiated and irradiated materials, respectively. Typical data is exhibited in Figure 2-2 from Roberts et al. (1979) [18] and Figures 2-3 and 2-4 from Brunisholz and Lemaignan (1987) [22]. The latter data was obtained for as-received Zr-4 17x17 stress-relieved and re-crystallized cladding samples. The differences in the data between the two lots in Figures 2-3 and 2-4 are due to differences in texture and heat treatment, but the

threshold values for both lots are 300 MPa for specimens with no fatigue-induced starter cracks. Pre-cracked specimens will be discussed in the next sub-section in connection with the effects of inner surface flaws. Applying the 2/3 factor, from Roberts et al. [18], to Brunisholz and Lemaignan data [22] to account for irradiation effects, the threshold stress is also 200 MPa. For the limiting case of a 17x17 configuration, with an oxide thickness of 100 μm, the cladding hoop stress is conservatively calculated to be less than 150 MPa. This is well below the threshold value of 200 MPa for irradiated Zr-4.

Effects of Irradiation/High Burnup

The effects of irradiation and high burnup on the cladding's susceptibility to SCC involve three important factors: irradiation hardening, hydrogen content and hydride morphology, and inner-surface flaws. The data of Roberts et al. [18] indicates that the effect of irradiation is to reduce the threshold stress by a factor of 2 for Zr-2, from 360 MPa to 180 MPa, and by a factor of 1.5 for Zr-4, from 300 MPa to 200 MPa. However, Videm and Lunde [38] show the opposite trend, with irradiation raising the SCC stress threshold for Zr-2 by 50 MPa at 340°C. No explanation was given by Videm and Lunde, other than the inference that their data was free of starter cracks that could have formed during irradiation. However, data by other workers (Cubicciotti and Jones [39]) is closer to the Roberts et al. data. Using the results of Roberts et al. [18] and Brunisholz and Lemaignan [22], 200 MPa is considered to be the appropriate value for the threshold stress of irradiated Zr-4.

As to the effects of hydrogen, the experimental evidence is that no synergistic enhancement of SCC susceptibility exists; in fact, the effect is the opposite. Sejnoha and Wood [40] found that hydrogen can retard crack initiation, changing the failure mode from transgranular cleavage to intergranular cracking. This was attributed to the blunting of the crack tip by the hydrides precipitating at the crack tip, and/or the increase in surface pitting to the exclusion of localized cracking. Similarly, Cox [41] found that deliberate precipitation of radial hydrides in a previously resistant batch of material did not render it susceptible to iodine-induced SCC. Further, he argued that pre-existing radial hydrides in susceptible material go into solution on raising the temperature at the start of the SCC test and the small cracks left behind act as initiation sites. However, he found no distinct separation between susceptible tubing containing radial hydrides and other susceptible tubing not containing radial hydrides. Thus, it can be concluded that the effect of hydrogen on SCC susceptibility is either neutral, or results in a slight improvement.

As to the third factor affecting SCC initiation, namely, pre-existing inner surface cracks, the experimental evidence is a reduction in both the threshold stress and the time to failure. The Brunisholz and Lemaignan [22] data for fatigue pre-cracked specimens shows that the apparent effect of pre-cracking is to reduce the threshold stress from 300 to 180 MPa, for unirradiated stress relieved Zr-4. It should be noted, however, that the fatigue pre-cracking virtually eliminated the need for a long incubation time, and as soon as iodine had sufficient time to diffuse to the crack tip, cracks with sufficiently high K_I, i.e., sufficiently deep cracks, began to extend almost immediately. Shorter cracks required longer incubation time, which is determined by the state of stress at the crack tip. Brunisholz and Lemaignan report that sharp fatigue-induced starter cracks of lengths up to 30% of the cladding thickness were found not to propagate

at all. From crack propagation analysis of their data, they were able to determine a K_{ISCC} value in the range 3.4-5.5 MPa$\sqrt{m}$, which is a factor of 2 lower than data by Wood et al. [42]. Brunisholz and Lemaignan compared their K_{ISCC} values to those obtained by Jones et al. [43] and Videm et al. [44], with 4.6 MPa$\sqrt{m}$ and 4 MPa$\sqrt{m}$ respectively. These values are more in line with the average of the Brunisholz and Lemaignan data of 4.45 MPa$\sqrt{m}$. More typical fracture toughness values for unirradiated Zircaloy in iodine vapor are in the range 7-10 MPa$\sqrt{m}$ (see Sejnoha and Wood [40], and cited references in their paper). It should be noted, however, that the basis for calculating K_{ISCC} is the edge-crack plate formula $K_{IC} = f \sigma (\pi a)^{1/2}$, where σ is the stress, a is the crack size and f is a constant that depends on the crack size. Aside from the fact that this formula is strictly applicable to a flat plate under plane strain condition, and, therefore, is misapplied to a tubular geometry, large errors may be introduced in the K_{ISCC} calculations because of errors in estimating the crack size. This may account for the variation in the fracture toughness values reported by the various authors.

Pre-existing flaws can be separated into two groups: short sub-critical ($K_I < K_{ISCC}$) cracks and deep ($K_I \geq K_{ISCC}$) cracks. As already mentioned, Brunisholz and Lemaignan [22] have found that fatigue cracks 160 μm deep did not propagate in iodine vapor, 200-μm cracks extended 30 μm, and 240-μm cracks led to fracture in 2.25 hours. The 160-μm value can be conservatively assumed to be the critical crack size, which, in a 17x17 configuration, is about 28% of the cladding thickness. Using their K_{ISCC} value, namely, K_{ISCC} = 3.4 MPa$\sqrt{m}$, which, as already discussed, is a factor of 2 lower than the prevailing values in the literature, an upper bound estimate of the crack size that could have existed in-reactor can be estimated. The upper-bound crack size is one that just remains sub-critical during a power ramp that would produce a PCMI stress increment equal to the SCC threshold stress of 200 MPa. Using the same formula used for calculating K_I, namely, $K_I = f \sigma (\pi a)^{1/2}$, with a shape factor f = 1.12 for an elliptical surface crack, and a = 160 μm, gives a K_I value of 5.0 MPa$\sqrt{m}$, which exceeds the K_{ISCC} value. This means that a partial crack of this size could not have remained sub-critical in-reactor, and therefore would not have pre-existed in spent fuel rods placed in dry storage.

Using a K_{ISCC} value of 3.4 MPa$\sqrt{m}$, and an applied stress equal to the threshold stress of 200 MPa, the maximum sub-critical crack size would be 73 μm. Such a crack size would represent the largest that can be assumed to pre-exist in a spent fuel rod in dry storage. Now, if we take the 150-MPa stress referred to earlier as deriving from the highest possible internal pressure, we calculate a stress intensity factor of 2.54 MPa$\sqrt{m}$, which shows that the crack will remain sub-critical during dry storage. These estimates are highly conservative, since the lowest SCC threshold stress, the lowest K_{ISCC} value, the highest rod pressure, enhanced cladding stress due to oxide-induced thickness loss, together with disregarding the blunting effect of hydrogen, have been used. This leads us to conclude that no enhancement of SCC susceptibility due to pre-existing flaws is possible and, further, any flaws that may have pre-existed are not subject to propagation by the SCC mechanism in spent fuel placed in dry storage.

Summary

The combined effects of the three areas examined above can be summarized as follows:

(1) Extrapolation to dry storage of the in-reactor chemical environment, which promotes PCI failures under very restrictive conditions, to spent fuel is not supportable by the laboratory simulations, and is unlikely to be operative under dry storage conditions.

(2) Under the most restrictive conditions, the stress in the cladding remains below the SCC threshold stress.

(3) High-burnup-induced damage, such as irradiation hardening, hydrogen and inner surface cracks are shown to be insufficient factors for increasing SCC susceptibility during dry storage.

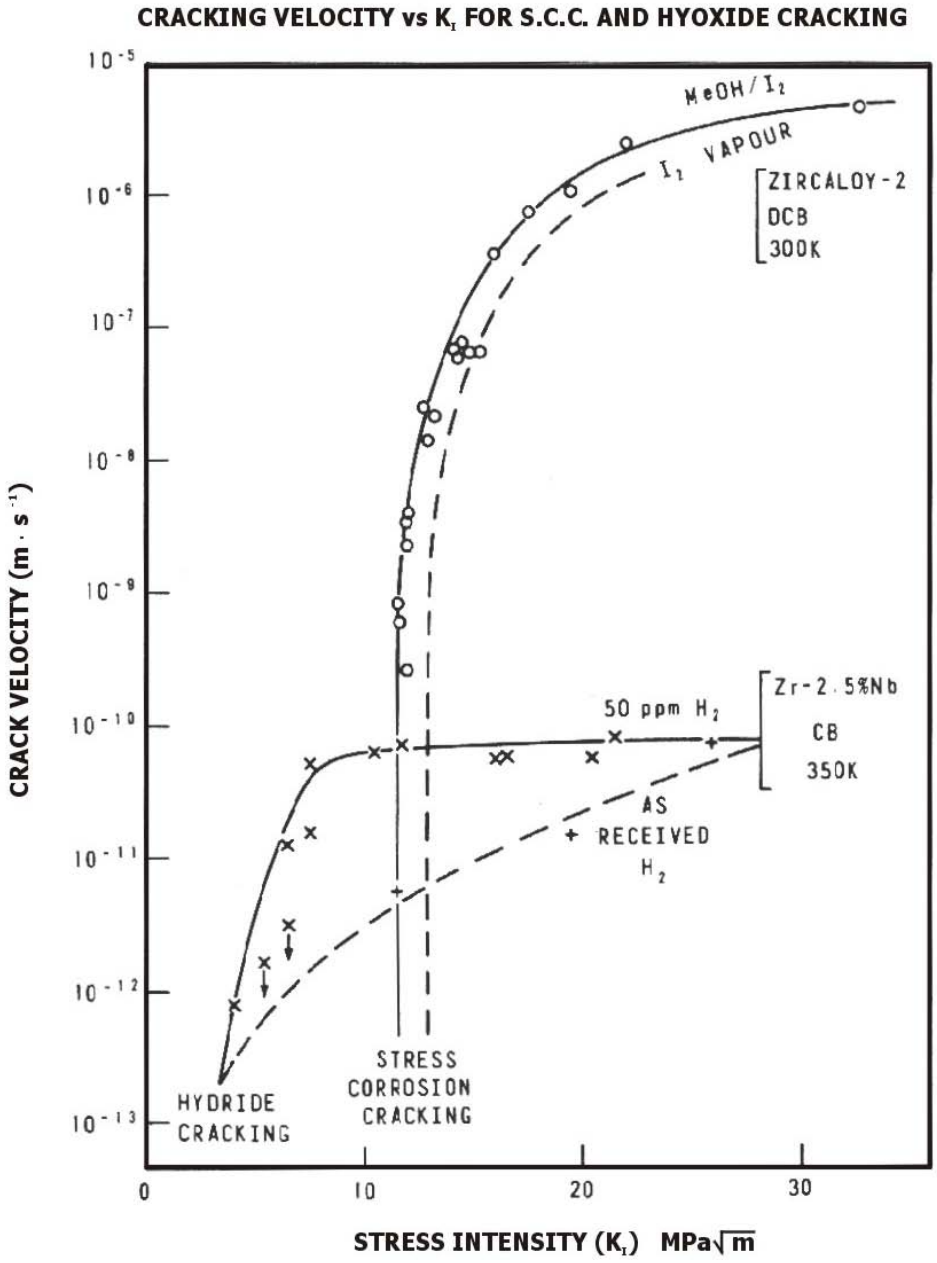

Figure 2-1. Crack Velocity versus Stress Intensity Curves for DHC and SCC (Ref. 41)

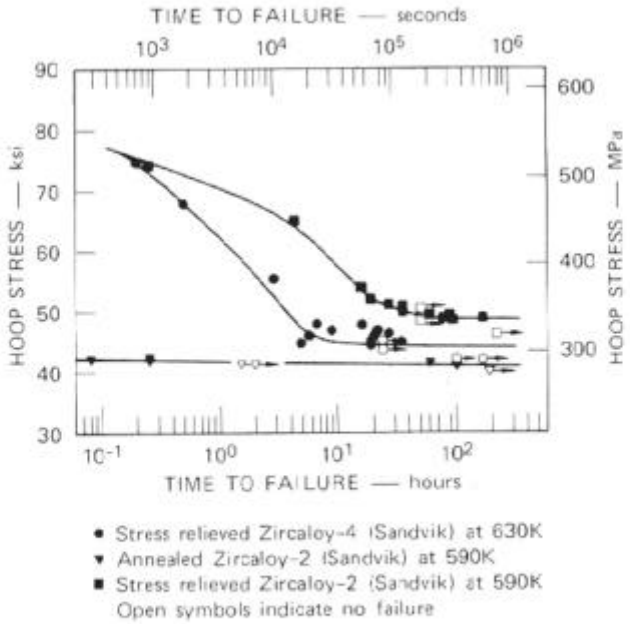

Results of Iodine-SCC tests at ~ 600 K on internally pressurized tube specimens of unirradiated Zircaloy-2 and Zircaloy-4

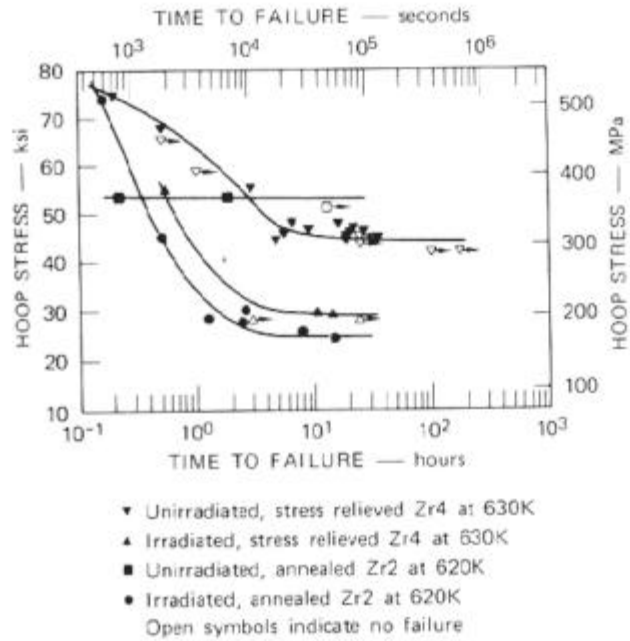

Effects of irradiation on the resistance of internally pressurized Zircaloy tubes to iodine-induced failure at ~ 600 K

Figure 2-2. SCC Data for Unirradiated and Irradiated Zircaloy at 600K (Ref. 18)

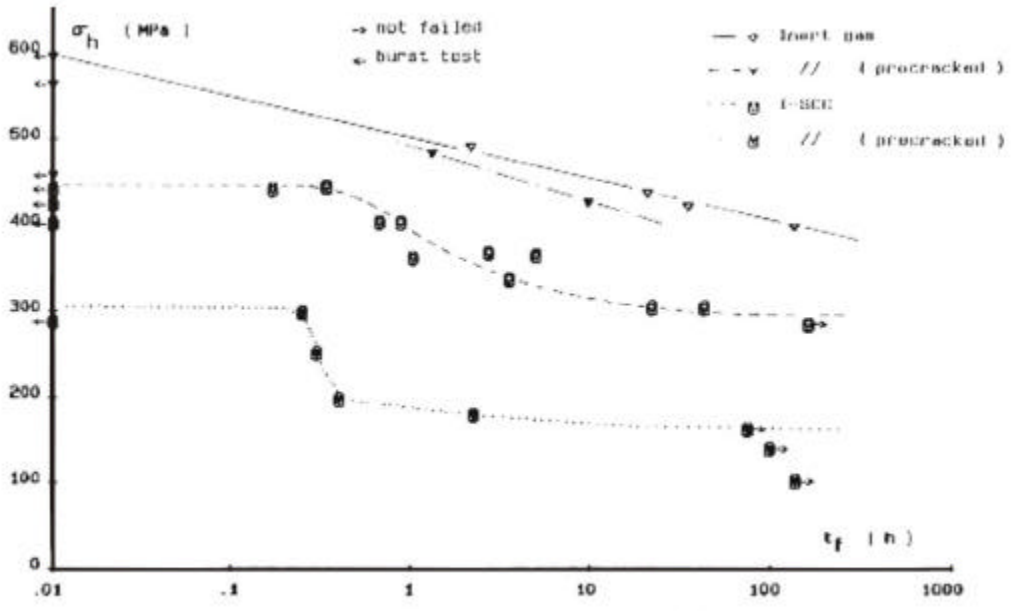

Figure 2-3. Time to Failure for Stress-Relieved Zircaloy-4 at 350°C (Ref. 22)

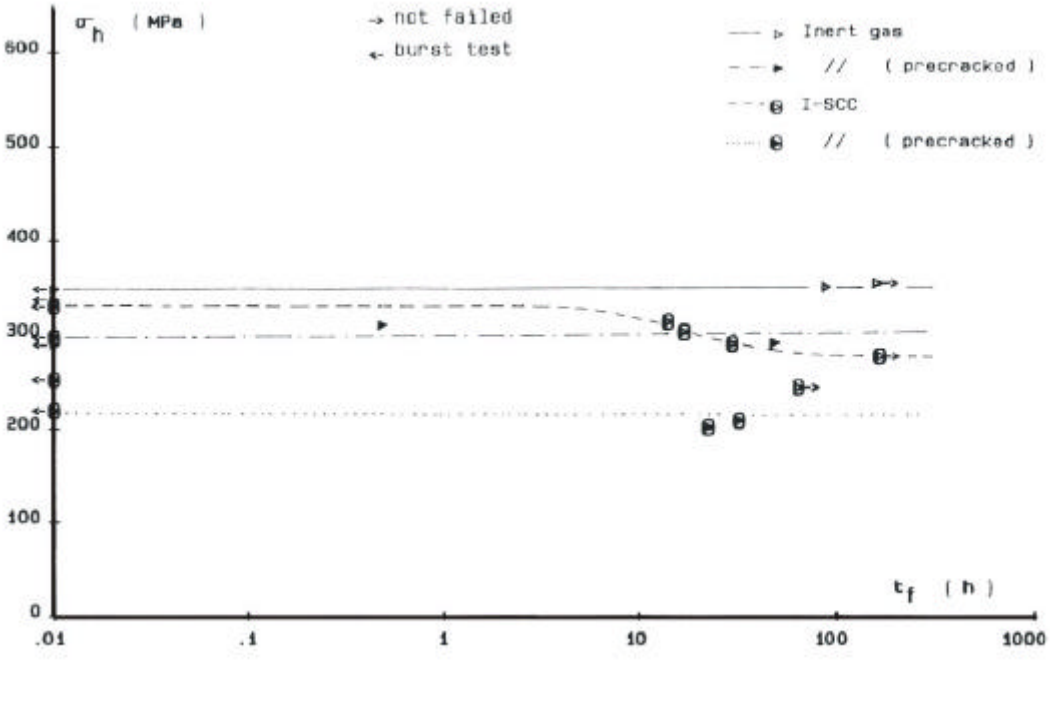

Figure 2-4. Time to Failure for Recrystallized Zircaloy-4 at 350°C (Ref. 22)

3

DELAYED HYDRIDE CRACKING (DHC) MECHANISM

Background

Delayed hydrogen cracking (DHC) failures of practical interest were first observed in the welds of experimental fuel elements (Simpson and Ells, 1974 [45]) and later in pressure tubes in the Pickering CANDU reactor (Ross-Ross, et al. [46]). Significant research was carried out in the succeeding years, although not to the same degree as in SCC, to study the DHC susceptibility of pressure tube materials, Zr-2.5Nb and Zr-2 (Dutton and Puls [47], Coleman and Ambler [48], Simpson and Nuttal [49], Simpson and Puls [50], Huang and Mills [51], Efsing and Petterson [52]). Except for the Zr-2 data cited above, no DHC data can be found for Zr-2 or Zr-4 cladding materials. This may be due to the fact that the DHC mechanism, unlike the SCC mechanism, was not implicated in the PCI failures that occurred in about the same time frame. Neither has there been any evidence of in-reactor fuel-rod failures attributable to DHC. (It should be noted parenthetically, however, that DHC was first thought to be the operative mechanism in the long axial splits of zirconium-lined BWR cladding, but the failures were shown to be the result of secondary hydriding (EPRI [53]). The lack of data on Zr-4 makes the present discussion applicable only by implication to PWR spent fuel in dry storage. Therefore, no attempt will be made in the present report, neither is one possible, to distinguish between the DHC susceptibilities of Zr-2 and Zr-4 cladding types, other than by inference that can be drawn from the calculated parameters. However, since all Zircaloys form hydrides, there is no reason to doubt the general validity of the DHC data or draw a distinction between the various materials' susceptibilities to DHC. As in the case of SCC, the DHC mechanism is dependent upon several forcing functions that affect spent fuel rod susceptibility to DHC failures, which are hydrogen, stress, and temperature, with time as the common independent variable. These are discussed in some detail below, but first it is relevant to give a brief description of the DHC mechanism, keeping in mind the ultimate objective of application to spent fuel dry storage.

Evolution of the DHC Mechanism

As the name implies, delayed hydride cracking is the slow evolution of failure as a result of hydride-induced embrittlement of the Zircaloy component. The prerequisite for this mode of failure is the presence of hydrogen in excess of the terminal solid solubility in combination with high internal stress. The hydrogen and the stress must interact in a specific manner under the appropriate thermal environment before the DHC process can be initiated. Laboratory tests of notched and pre-cracked specimens show that the process evolves in two stages. Stage-I is comprised of crack initiation followed by a rapid increase in crack velocity, of one or two orders of magnitude, until it transitions to the stable crack growth Stage-II. This latter stage controls the time to failure. The reported data is depicted as plots of crack velocity vs. stress intensity factor K_I, Figure 3-1, and K_I vs. time to failure, Figure 3-2.

The failure time is determined primarily by the nearly constant crack growth velocity of Stage-II, which is initiated at a K_I value around 9-10 MPa$\sqrt{m}$, compared to the threshold value of 5-6 MPa$\sqrt{m}$ for K_{IH}, which initiates Stage-I. During Stage-II, under isothermal conditions, the hydrogen in solution diffuses to the high stress zone surrounding the crack tip. An important condition that promotes the diffusion of hydrogen to, and the precipitation of hydrides in, the crack tip zone is the triaxial tensile field surrounding the crack tip. This condition exists in the plane strain test specimens that are machined from thick pressure tubes. This is an important point to consider when applying the data to the plane-stress cladding geometry in which the crack tip stress field is biaxial, and therefore is not as attractive to hydrogen. With the continuous hydrogen diffusion to the crack tip region, the local hydrogen concentration rises until it exceeds the solubility limit and hydrides begin to precipitate ahead of the crack tip in the form of platelets oriented perpendicular to the direction of the stress. When the hydride reaches a critical size, it fractures, allowing the crack to advance until it is arrested in the tougher Zircaloy material past the hydride, where a new highly stressed crack tip is formed, and the process is repeated. The crack continues to propagate in this intermittent manner until failure by the plastic instability of the remaining ligament. This process is illustrated in Figure 3-3.

Role of Hydrogen

One of the distinguishing features of the DHC mechanism is that there is no threshold value for the amount of hydrogen in the material, as long as it is in excess of the solubility limit. The process, as the data indicates, can occur in as-received material under the appropriate temperature and stress conditions. Thus, since hydrogen is abundant in spent fuel cladding, especially at high burnup, the DHC process is not constrained by hydrogen availability.

Role of Temperature

Temperature and prior temperature history play a crucial role in the DHC process, affecting the two stages in different ways. The first stage was found to be weakly dependent on temperature. This means that a necessary and sufficient condition for Stage-I to be initiated is $K_I \geq K_{IH}$, where K_I is dependent only on the far-field stress and the crack size, and K_{IH} is independent of temperature for Zr-2.5Nb, but may be slightly sensitive to temperature for Zr-2. The second stage, on the other hand, depends on the direction of approach to temperature, as will be discussed further below.

The crack growth rate in the second stage, which determines the failure time under DHC, is governed by the hydrogen diffusion rate, which is strongly temperature dependent. Consequently, the crack velocity follows a simple thermally activated process, i.e., $V = Ae^{-Q/RT}$, with Q = activation energy. Coleman and Ambler [48] determined a value for Q = 42 KJ/mol, whereas Simpson and Puls [50], using a more reliable, multi-specimen approach determined a value for Q = 65.5 KJ/mol. It is interesting to note that the Simpson and Puls value is close to the theoretical activation energy of hydrogen diffusion of 69.5 KJ/mol. Huang and Mills [51] determined an activation energy value for Zr-2, which is in agreement with the Simpson and Puls value for Zr-2.5Nb. The overall temperature dependence of Stage-II is summarized below.

In the laboratory, the DHC process was found to depend on the direction of approach to test temperature, i.e., whether the test temperature was approached from above or from below. A critical temperature, termed T_{DAT} (Direction of Approach to Temperature), was found such that at a test temperature below T_{DAT}, DHC occurred always regardless of whether the material was heated or cooled to the test temperature. However, above T_{DAT}, DHC occurred at constant or decreasing temperature, but only when the test specimen was first subjected to a temperature cycle with an over–temperature excursion in the range of 20-40°C. Even a propagating crack at a temperature above T_{DAT} could be arrested completely by a small temperature increase. T_{DAT} was found to be 150°C for Zr-2 plate and 180°C for Zr-2 tubing (Huang and Mills [51]).

The crack velocity differs significantly above and below T_{DAT}. Below T_{DAT}, the crack growth rate follows the Arrhenius relationship described above; whereas at temperatures above T_{DAT}, the constant-temperature crack velocity decreases rapidly, but maintains the Arrhenius rate on cool-down, which is the prevailing condition in dry storage.

Providing that stress conditions are satisfied (see below), it would appear from the above that the temperature history in spent fuel would not preclude DHC. The slowly decreasing temperature with time during dry storage is almost the ideal recipe for maintaining crack propagation, provided of course that Stage-II had already been initiated. Therefore, the key is to prevent Stage-II from initiating by precluding Stage-I altogether. This is explored in the following sub-sections.

Role of Stress - DHC Initiation

Stage-I of the DHC process can be initiated in a fuel cladding if and only if the far-field hoop stress can produce a K_I value in a pre-existing crack of sufficient size such that the condition $K_I \geq K_{IH}$ is satisfied. This requires knowledge of three quantities, the fracture toughness K_{IH}, the far field stress, and the crack size. The role of these parameters on DHC initiation is examined below for the two cladding conditions, namely, coherent oxide, i.e., no delamination or spallation, and spalled oxide. But, first, we need to compare the fracture toughness K_{IC} with the DHC fracture toughness K_{IH} for both oxide conditions to determine which fracture mode governs. This requires an estimate of K_{IC} for spent fuel cladding. This is obtained below.

K_{IC} Estimation from Material Properties Data Using the CSED Model: K_{IH} is already known from the earlier calculations; an estimate of K_{IC} is needed. For this, two different types of data sets, fracture data by Kreyns et al. [54] and material property data by Garde et al. [55], together with an analytical model that relates the two types of properties, are used. The analytical model is the critical strain energy density (CSED) developed elsewhere. (For a detailed discussion on the application of the CSED concept to fuel cladding failure evaluation, see EPRI's RIA report: EPRI TR-106387, August 1996 [56]; and also Rashid et al., IAEA Specialists Meeting on Fuel Modeling, Windermere, June, 2000 [57].) The following relationship between CSED and the fracture toughness K_{IC}, namely, $K_{IC} = 3.5\sqrt{CSED}$, was developed semi-analytically and was shown to apply to a wide variety of conditions (see Rashid, "Fracture Toughness Data for Zirconium Alloys - Application to Spent Fuel Dry Storage, EPRI report in preparation [58]).

Figure 3-4 shows the CSED as function of oxide thickness developed from material property tests by Garde et al. and others [55,56]. The figure includes unspalled and spalled data with best-fit curve for each. Using the above K_{IC}-CSED correlation and the unspalled best-fit CSED value of 5 MPa at an oxide/cladding thickness = 0.25 from Figure 3-4, a fracture toughness K_{IC} = 7.8 MPa$\sqrt{m}$ is obtained. The 25% oxide thickness used in the above calculation is equivalent to 1216 ppm for the 710-μm thick cladding used at Calvert Cliffs-1 (CC-1). This was estimated from the following hydrogen-oxide thickness correlation [59]:

$$H\ (ppm) = 7.18 * X\ (\mu m) - 58.4$$

Kreyns et al. [54] used hydrogen-charged irradiated and unirradiated test samples under various temperatures, They reported fracture toughness value as low as 7.4 MPa$\sqrt{m}$ for unirradiated samples with 4000 ppm hydrogen tested at 24°C. There are differences in the material behavior between hydrogen-charged samples and fuel rods because of differences in hydride distribution and morphology. Comparing the 7.4 MPa$\sqrt{m}$ value from the Kreyns et al. data at 4000 ppm with the 7.8 MPa$\sqrt{m}$ estimated for Garde et al.'s data at 1216 ppm, indicates a penalty factor of approximately 3 (4000/1216 = 3.3) on the hydrogen-related damage between artificial hydrogen and oxide hydrogen.

As a further validation check on the use of the K_{IC}-CSED correlation and the effects of hydrogen, the correlation is applied to Kreyns's et al. irradiated samples with a charged-hydrogen content of 1600 ppm. The samples were tested at temperatures in the range of 204°C, with a measured K_{IC} of 13.3 MPa$\sqrt{m}$. The CSED value that corresponds to K_{IC} = 13.3 MPa$\sqrt{m}$ is calculated from the K_{IC}-CSED correlation to be 14.5 MPa. This corresponds to an oxide thickness of 11% from Figure 3-4, or about 80 μm for CC-1 cladding and 70 μm for ANO-2 cladding. The average hydrogen concentration corresponding to an oxide thickness of 80 μm, as obtained from the hydrogen-oxide correlation, is 516 ppm. The penalty factor is 1600/516 = 3.1, which is sufficiently close to the factor of 3. This analysis serves as a transfer function between the two types of data and allows us to apply the results to the two oxide conditions.

<u>*Cladding with Coherent Oxide*</u>: From the above calculations, the K_{IC} values for spent fuel cladding with coherent oxide can vary from 13.3 MPa$\sqrt{m}$ for cladding with an oxide thickness of 80 μm to 7.8 MPa$\sqrt{m}$ for an oxide thickness well in excess of 100 μm. These values are higher than the threshold K_{IH} in the range 5-6 MPa$\sqrt{m}$ for irradiated Zr-2 from Huang and Mills [51], and for Zr-2.5Nb from Simpson and Puls [50]. In Section 2, we have already estimated the upper bound of the size of an inner-surface crack, the far-field stress and the stress intensity factor K_I to be respectively 73 μm, 150 MPa and 2.54 MPa$\sqrt{m}$. These estimates indicate that the maximum pre-existing inner-surface crack, if it exists, would remain sub-critical with respect to both mechanical fracture and DHC Stage-I initiation.

<u>*Cladding with Spalled Oxide*</u>**:** Cladding with spalled oxide can develop hydride lenses in the newly exposed colder region of the cladding. The maximum penetration of these hydride lenses observed in high burnup cladding is close to cladding mid-wall. If we examine the individual data in Figure 3-4, we see that the CSED for spalled rods tested under internal pressure is about 4 MPa, which gives a K_{IC} of 7 MPa$\sqrt{m}$. The average hoop stress for the specimen is roughly 480

MPa from Reference [59], which results in a critical crack size of 55 μm. This represents the maximum crack that can pre-exist in a cladding with spalled oxide. A spent fuel rod with this condition would sustain a stress in the ligament of 265 MPa based on a far-field stress in the un-spalled region of 150 MPa. This gives a K_I value of 3.9 MPa$\sqrt{m}$, which is well below K_{IH}. This shows that the inner-surface crack of 73 μm is the governing condition. If we assume further that such a crack is located on the ID side of the hydride lens, we calculate a K_I of 4.5 MPa$\sqrt{m}$, which is still below K_{IH}.

We have so far concentrated on the stress conditions that are needed to initiate Stage-I, and found those to be lacking even for cladding with spalled oxide. The crack-growth process, however, is governed by the conditions for Stage-II. The overwhelming evidence from the literature sources already cited is that a K_I value of at least 9-10 MPa$\sqrt{m}$ is needed to sustain crack growth in Stage-II. Since crack-growth during the transition from Stage-I to Stage-II is negligibly small, the K_I value of 4.5 MPa$\sqrt{m}$ calculated above for cladding with spalled oxide remains valid. As can be seen, this is half the value needed to initiate Stage-II and subsequently sustain crack growth.

As a cautionary note, we should mention that these hand calculations push the K_I formula to the limit of validity, and ultimately more precise calculations can be made, if necessary. However, by virtue of the conservative assumptions made for the various parameters, the present conclusions should not be affected.

Role of Hydrides Re-orientation

Hydrides reorientation from tangential to radial was created in the laboratory by repeated thermal cycling of test samples subjected to high tensile stress (Simpson et al. [60]). If the hydrogen content of the sample exceeded the terminal solid solubility at the high temperature level of the cycle, the number of re-oriented hydrides increased with every cycle. Simpson et al. found that a stress in excess of 138 MPa was required, and the degree (number and angle) of re-orientation was strongly dependent on the number of cycles, with tens of cycles required to produce significant re-orientation. Hydrides orientation is texture dependent, and, consequently, changes in texture as a result of temperature and stress can produce re-orientation of hydrides at different stress levels depending upon the temperature: the higher the temperature, the lower the stress needed to cause re-orientation. For example, at 400°C the stress level required to cause hydrides re-orientation is in the range of 120-180 MPa, and at 250°C the required stress is 250-350 MPa, Peehs et al. [76], Hardie and Shanahan [77]. These stresses are predominantly outside the range of spent fuel storage conditions.

There are two opportunities where hydrides re-orientation can occur in spent fuel: during vacuum drying and during long-term storage under the slowly decreasing temperature. During long-term storage, the continuous drop in rod pressure due to the drop in temperature and the creep-induced volume expansion will cause the cladding stress to drop within the first year or so below the threshold value. As the threshold value increases with temperature, this further reduces the chance for re-orientation. Also, the number of hydrides that will precipitate will be limited to the reduction in the solid solubility limit over this period. It should be reminded, further, that the 150-MPa stress is an upper bound estimate, not the actual that might exist. The number of

thermal cycles to which spent fuel may be subjected during vacuum drying is minimal in comparison with laboratory data, and therefore we can ignore the cumulative effect of thermal cycling. However, since the cladding threshold stress for hydrides re-orientation may be exceeded, we cannot rule out the presence of some radial hydrides following vacuum drying. Limiting the drying temperature may reduce the number of tangential hydrides that dissolve and subsequently re-precipitate in the radial direction during cooling, but such a step may not be necessary. The experiments performed by GNB/Siemens (W. Goll, E. Toscano, and H. Spilker, KTG "Brennelemente und Kernbauteile, Karlsruhe, Feb 29-Mar 1, 2000 [61]) showed limited re-orientation even for cladding that was cooled down after being maintained at high temperature and pressure for several days. However, in view of the fact that the process cannot be ruled out since there is no threshold temperature for hydrides re-orientation, resolution of the situation effectively comes down to the role of the stress, which is discussed next.

There are two ways in which hydrides re-orientation interact with the stress in the cladding. First, the hydrides may inter-link and form long radial hydrides. In the presence of internal loading, pressure or PCMI, the worst position for such a long hydride is at the inner surface where the stress is highest and can create an edge crack which acts as a starter crack for Stage-I DHC. However, internal long hydrides can also crack given sufficiently high stress. Once the crack is initiated, and is sufficiently deep such that the stress intensity factor K_I exceeds the fracture toughness K_{IH}, the crack advances with increasing velocity until the onset of Stage-II, as already discussed. To determine if Stage-I can be initiated from a fractured hydride, we first have to estimate the length of the hydride that can fracture under 150-MPa stress, which is the maximum stress that has been assumed to exist (see Section 2). The fracture toughness of a pure zirconium hydride is in the range of 1-3 $MPa\sqrt{m}$. Using these values, we calculate the critical hydride length to be in the range of 11 μm to 102 μm, with a mid-range value of 45 μm. Simpson et al. [60] found that hydrides of 100 μm in length fractured under a stress of 560 MPa, but hydrides of 25 μm in length did not. By comparison, under 150-MPa stress, the fracture of the 102-μm hydride would be unlikely. However, even if a hydride of this length can exist and fractures under a stress of 150 MPa, the resulting crack is sub-critical with respect to the DHC and SCC fracture mechanisms. The stress intensity factor K_I for a 102-μm crack under 150-MPa stress is 3 $MPa\sqrt{m}$, as compared to K_{IH} of 5 $MPa\sqrt{m}$ and K_{ISCC} of 3.4-5.5 $MPa\sqrt{m}$.

The second way in which hydrides re-orientation interact with the stress is when cracks or notches pre-exist in the cladding. The biaxial tension field of the crack tip will attract the hydrides and cause them to concentrate in the process zone of the crack tip. Simpson et al. [60] have demonstrated hydride cracking in Zr-2 round-notched bar specimens at calculated stress intensity factor of 5 $MPa\sqrt{m}$ after up to 240 thermal cycles between 300 and 60°C. Such thermal cycling is well beyond spent fuel storage experience. Moreover, we have shown in our previous calculations that for a 5-$MPa\sqrt{m}$ value for K_{IH}, a conservatively estimated pre-existing crack of 73 μm does not propagate. In summary, hydrides reorientation is shown to be of benign consequences for dry storage.

Summary

Certain elements of spent fuel dry storage are conducive to promoting DHC. More importantly the factors that render the process inoperative dominate spent fuel conditions in dry storage.

Elements conducive to promoting DHC are the availability of hydrogen in excess of the terminal solid solubility, the possible presence of inner and outer surface flaws that form starter cracks for Stage-I DHC, and the cladding temperature history. The troublesome, but unavoidable, aspect of the temperature history, which makes it particularly suited for promoting DHC, is the over-temperature excursion during vacuum drying, with possible cycling, followed by a continuously decreasing temperature.

However, DHC cannot begin without the appropriate stress condition being satisfied, regardless of any other promoting mechanism. The stress environment is shown to be non-conducive to DHC using highly conservative assumptions on the parameters that govern DHC initiation and cladding condition. These are: maximum far-field stress, largest possible pre-existing crack size in combination with spalled oxide with hydride lenses, a 100-μm oxide thickness, the lowest hydrogen-assisted fracture toughness value K_{IH}, and a conservative estimate of the stress intensity factor K_I needed to sustain Stage-II crack growth.

A most revealing result from the present investigation is that hydrides re-orientation, and its possible impact on the initial drying temperature, is found to present little additional concern and does not impose undue restrictions on vacuum drying.

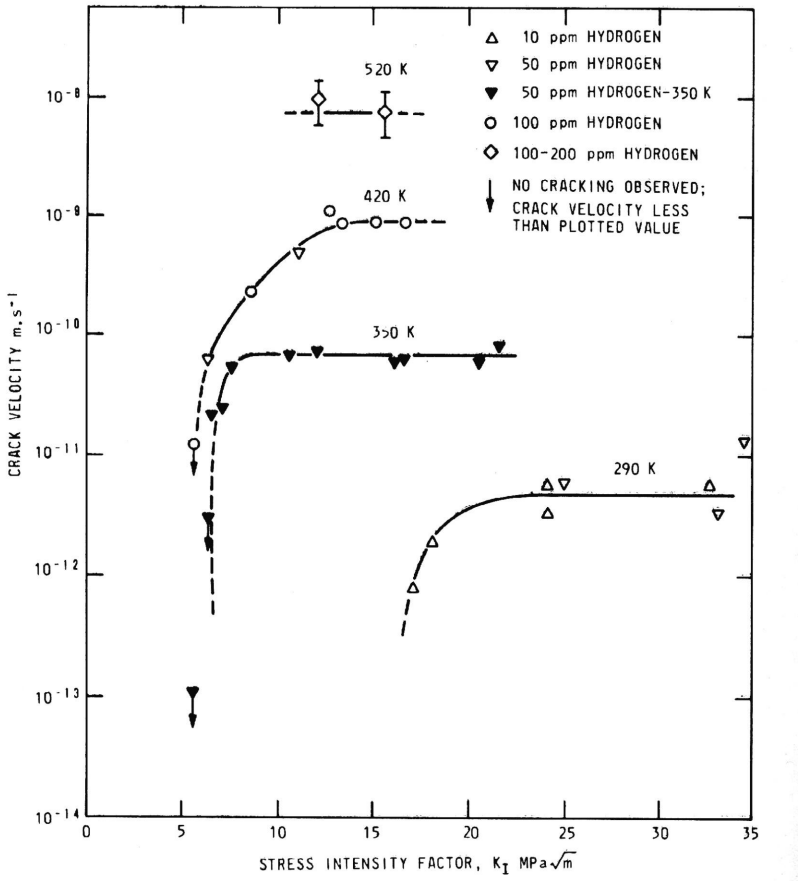

Effect of K_I on crack velocity in notched cantilever beams of cold-worked Zr-2.5Nb.

Figure 3-1. Crack Velocity versus Stress Intensity Factor K_I (Ref. 48)

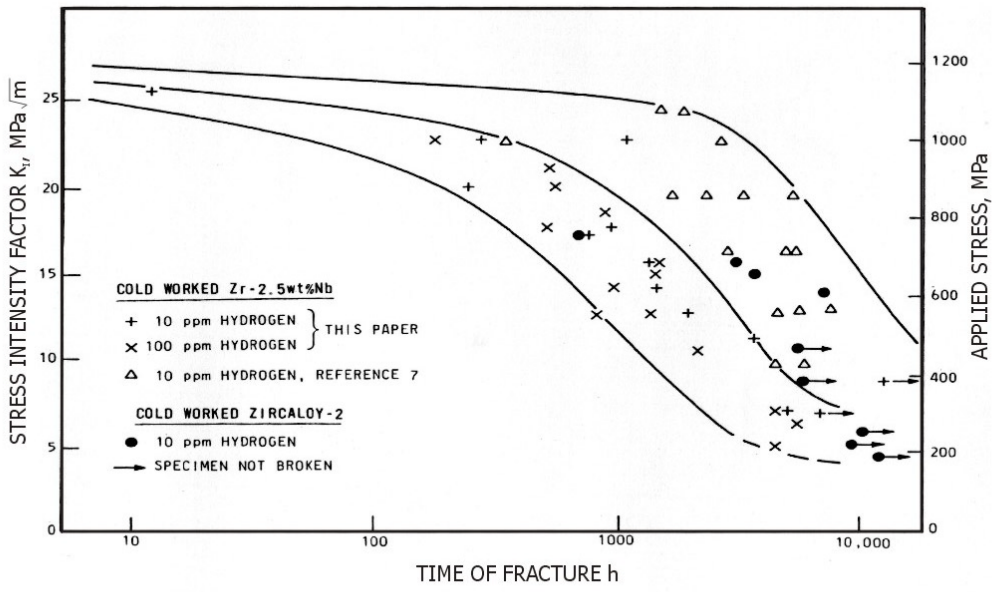

Effect of K_I on time to failure in round notched bars at 350K.

Figure 3-2. Stress Intensity Factor K_I versus Time to Failure (Ref. 48)

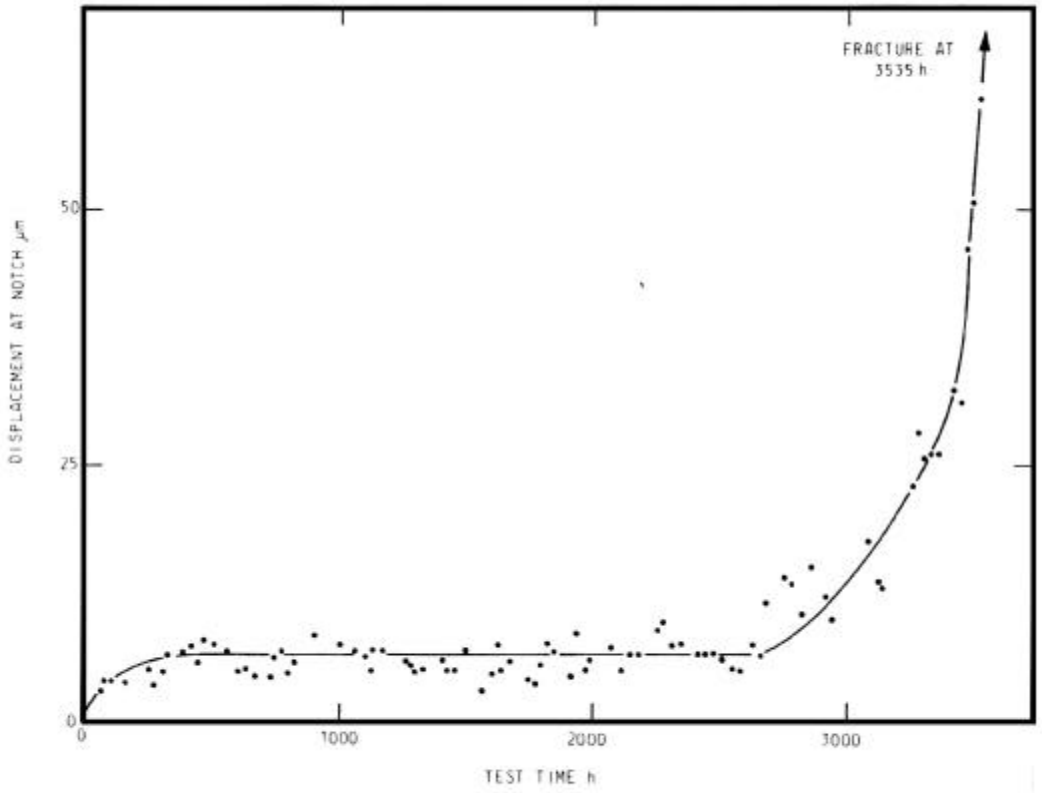

Displacement-time curve for round notched bar of Zircaloy-2 containing 100 ppm hydrogen and tested at 350 K with K_I *of 15 MPa* $\sqrt{m}$.

Figure 3-3. Intermittent DHC Crack Evolution (Ref. 48)

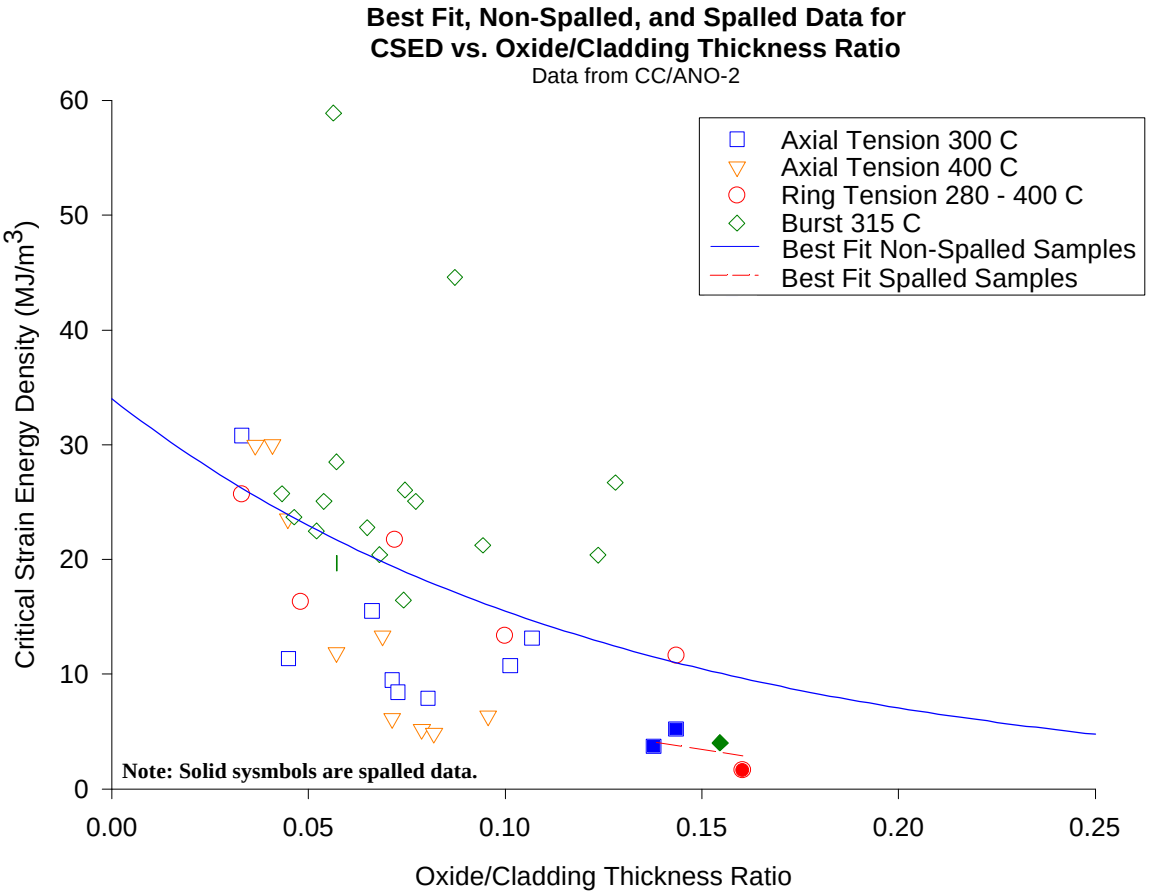

Figure 3-4. Critical Strain Energy Density (CSED) Data for High-Burnup Fuel Rods

4

CREEP MECHANISM

Background

Spent fuel rods in dry storage undergo creep deformations at a rate determined by two opposing processes. One process is the material's tendency to steadily deform at a constant rate following a short period of transient creep, and the other is the material's reaction to continuously decreasing pressure and temperature. The latter imposes a form of break mechanism on the former, eventually bringing the two processes into a state of near equilibrium where the deformation is halted or its rate is reduced to a negligible level. It can be shown analytically that such equilibrium state is the only possible outcome in a pressurized closed system. The question is: When in the history of the fuel rod does this state of near equilibrium occur and at what deformation level? This is governed by the creep capacity of the cladding, which will be examined in this section.

Before the advent of spent fuel storage, the emphasis has been on irradiation-enhanced thermal creep, which was mainly needed to calculate the effects of cladding deformations on the fuel-clad gap heat transfer. In PWRs, the process is primarily compressive creep, or creep-down, under constant power, with occasional excursions into the tensile strain regime induced by PCMI during power ramps. Towards the latter part of the burnup cycle, tensile strains could be induced under constant power at a very slow rate due to fuel swelling. The overall process is similar for BWRs, but with significant differences in strain magnitudes; for example, less creep-down but higher PCMI strains. Despite the apparent complexity of the deformation processes involved, in-reactor fuel rod response has been fairly predictable using fuel performance codes whose primary function is to calculate specific design limits (SAFDLs). The most notable of these SAFDLs is the 1% strain limit, which was initially arbitrarily chosen as a sufficiently safe limit for what was thought to be a rather benign loading regime, despite the fact that much larger strain limit could be justified. Unfortunately, however, the 1%-limit seems to have entered the annals of fuel behavior technology as a one-size-fits-all criterion.

Recent efforts to evaluate the cladding creep capacity in dry storage (Spilker et al. [69]) utilize creep data obtained for unirradiated cladding, with the hypothesis that the calculated strain would be conservatively judged against the 1% criterion. (Note that the elastic strain component decreases continuously with time, eventually becoming insignificant, and therefore no distinction needs to be made whether the 1% criterion is purely plastic or elastic plus plastic.) The first opportunity to test this hypothesis in the U.S. regulatory arena presented itself in the NRC review, performed by PNNL staff, of the license application of the Wesflex design (see Gilbert et al. [71] "Technical Evaluation Report of WCAP-15168, Dry Storage of High Burnup Spent Nuclear Fuel"). The reviewers accepted the 1% strain criterion, but restricted it to spent fuel cladding with oxide thickness below 70 μm. Cladding with 80 μm or higher oxide was to be

treated as damaged. They relied on burst data by Garde et al. [55] and Fuketa et al. [66] as supporting evidence. In arriving at their recommendations, Gilbert et al. applied literal interpretations of material properties data generated in standard tensile tests, ignoring well known effects that distinguish the low-stress low-rate creep regime from the more aggressive stress-strain tests. The elasto-plastic work done on the material in these tests can be a factor of 10 greater than the visco-plastic work done due to a 1% creep strain accumulated during dry storage. Asserting that the material's energy capacity is a fundamental invariant of material behavior, we would conclude that the strain capacity under creep is far greater than under short-duration loading. This is confirmed by Fuketa et al. [66] who point the difference out in their paper where loading rate differences are only three orders of magnitude instead of the six orders of magnitude under creep.

The apparent loss of ductility measured in stress-strain tests by Garde et al. [55], which was referenced in the Gilbert et al. [71] review of the Wesflex report was totally attributed to the hydrogen content and, by extension, to the oxide thickness. However, data by W. Goll et al. [61] ("Short-Time Creep and Rupture Tests on High Burnup Fuel Rod Cladding") and S. B. Wisner and R. B. Adamson [72] ("Combined Effects of Radiation Damage and Hydrides on the Ductility of Zircaloy-2") show that at temperatures of specific interest to high-burnup fuel storage, i.e., between 300° and 400°C, both Zircaloy-4 and Zircaloy-2 tubing retain ductility above 2.5-4%, when specimens are tested under conditions relevant to dry storage. Also, Jahreiff et al. [73] indicate that even up to 2000 ppm, hydrides do not decrease the ductility of irradiated Zircaloy. In the above-cited Wisner's and Adamson's work, in particular, it is clearly shown that radiation damage controls the ductility of Zircaloy-2 up to hydride levels of at least 800 ppm (see Conclusion 2 of Wisner and Adamson [72]). Curiously, however, Gilbert et al. quoted instead a value of 400 ppm from the same Wisner and Adamson paper to justify the 70-μm oxide limit [71]. It is interesting to note that the corresponding oxide thickness for 800-ppm hydrogen content is ~100 μm (see the hydrogen-oxide correlation in Section 3 of this report).

Creep Data

As already stated, in order to evaluate the creep capacity of the cladding under long term dry storage conditions, we need two types of information: applicable creep data, including creep rupture criterion, and an analytical model capable of simulating the cladding response under the prescribed temperature and pressure conditions. The type of creep data needed is post-irradiation thermal creep strain as function of stress, temperature and time. The creep rupture criterion, on the other hand, need not be a true rupture strain but rather a strain measure that recognizes the cladding physical conditions and loading rate, and has sufficient margin against instability or rupture.

A limited amount of out-of-pile creep data for irradiated material was generated in the eighties by German researchers [74,75]. That data, however, is not sufficiently complete or robust to enable the development of an analytical model for application to the dry storage of high burnup spent fuel. These data were generated to demonstrate that irradiated cladding creep rates are always lower than those of archive claddings in the unirradiated condition. Recent data by Limon et al. [63] was generated for irradiated Zr-4, from FRAMATOME fuel rods, under stress and temperature conditions somewhat above the range of spent fuel conditions. The burnup level

was approximately 47200 MWd/tU. The stress was in the range of 150-250 MPa, and the temperature was in the range of 380-420°C. The longest duration of the creep tests was roughly 1350 hours. Some of the data is shown in Figures 4-1 and 4-2. Limon et al. formulated a primary-creep model only, arguing that the data was not sufficient to allow the formulation of a secondary creep component. It is interesting to note, however, that the data could not produce a secondary creep term in spite of the fact that some of the tests were carried out to rupture, as shown in Figure 4-3. We will come to this point in later remarks.

The accelerated creep tests reported in Goll et al. [61] provide support for a 2% creep strain-limit criterion. In addition, the accelerated creep tests were followed by a lower temperature test at 150°C and hoop stress equal to 100 MPa to assess the long-term behavior of the cladding, and to examine the effects of decreasing temperature in the presence of tensile stress on hydride re-precipitation and re-orientation. During accelerated creep testing at 300°C, some of the hydride platelets were dissolved and re-precipitated under stress during cool-down to 150°C. This led to the precipitation of some radially oriented platelets. The cladding material was then held at 150°C and 100 MPa for as long as 5 days, without cladding failure. This result shows the ability of the sufficiently ductile zirconium matrix to immediately blunt cracks emanating from the radially oriented hydrides.

Gras et al. [64] developed a two-term creep equation in which the effect of prior irradiation was introduced as multipliers, functions of fast fluence, on the primary and secondary terms. The specifics of this model, however, are not in the open literature, as yet. The available data from Goll et al. cited earlier is not adequate to formulate a creep model, but can be useful for the validation of newly developed creep models. Data are expected to become available in the next 24 months from various organizations, including the current NRC/EPRI/DOE and NRC/EPRI testing programs at ANL. Until this additional data becomes available, the above-cited data may be all that can be currently used in the creep modeling and analysis of spent fuel rods in dry storage. It is possible, however, to employ analytical techniques to extrapolate thermal creep data to post-irradiation thermal creep. This is further explored in the next sub-section.

Choice of Creep Model

A comprehensive survey of creep of zirconium alloys in nuclear reactors is given in a Special Technical Publication of ASTM fully dedicated to the subject, authored by Franklin, Lucas and Bement, STP 815, 1983 [62]. Although the publication, which contains 279 references, is nearly two decades old, the statement in the book, "Despite the considerable research…., a full understanding of creep in these alloys is not yet in hand", is still true today. Therefore, it would be counterproductive to engage in a yet-another discussion (see Refs. [6] and [7]) to confirm or refute the applicability of the DCCG and CSFM methodologies to spent fuel storage. Rather, we would begin by stating that a properly characterized phenomenological creep model is appropriately suited for describing cladding time-dependent deformations during dry storage. This section will discuss the attributes of such a phenomenological model, its data needs, and how it can be used to evaluate the creep capacity of spent fuel in dry storage.

In general, a phenomenological creep model for Zircaloy cladding would express the creep strain as an algebraic equation comprised of individual terms each of which describes the contribution

of a single independent variable, namely, stress, temperature, neutron flux, fast neutron fluence and time. This is to be distinguished from mechanistic models, of the type used in the DCCG/CSFM methodology, which attempt to describe creep in terms of the interaction of structural defects such as vacancies, interstitials and dislocations, which involve extremely complex processes. A suitable phenomenological creep equation for post-irradiation thermal creep would have the following form:

$$\varepsilon^c = \varepsilon_p^c + \varepsilon_s^c \tag{1}$$

The subscripts *p* and *s* stand for primary creep and secondary creep respectively. Each of the terms in the above equation is a function of time and time-varying stress and temperature. In the absence of fast neutron flux, the effects of prior irradiation hardening is introduced as a multiplier lumped with the model constants. The primary and secondary creep components take on the following form:

$$\varepsilon_{p,s}^c = A * f_1(\sigma) * f_2(T) * f_3(t) \tag{2}$$

The parameter A is a constant multiplier, which contains the effects of prior irradiation hardening as a fast fluence term. The independent variables in the above equation vary throughout the history. Numerical implementation of creep models of this form should be done within the framework of the strain-hardening rule.

The temperature and time dependencies are straightforward, and most creep-model developers agree on their form. The time dependency is usually expressed as time raised to a power of less than one for the primary component and of unity for the steady state component. The temperature dependency is expressed as an Arrhenius term with the appropriate activation energy values for primary or secondary creep. The stress-dependency is somewhat more complicated, and has been the source of controversy. For a stress dependency of the type σ^n, the creep rate varies from linear, n = 1, to highly non-linear, n > 10. Mechanistic models divide the creep mechanism into various stages, depending upon the level of the stress. At low stress levels, e.g., less than 20 MPa, the value of *n* is close to unity, and the process is diffusion controlled. At intermediate and high stresses, the mechanism is dislocation controlled, where dislocation glide creep pre-dominates at intermediate stresses and dislocation climb-glide creep dominates at high stresses. Phenomenological models, on the other hand, express the stress dependency as σ^n, with n given different values depending on the stress level. A more convenient way of expressing the stress dependency is by using a hyperbolic sine function, which allows the stress dependency to vary automatically according to the stress level [63].

<u>*Use of Model to Extrapolate Thermal Creep Data to Post-Irradiation Creep*</u>: As was already mentioned, the stress exponent *n* increases with the stress and can reach very large values, of the order of 100, as the stress approaches the yield or ultimate strength. In fact, for non-strain-hardening materials, which approximately characterizes Zircaloy at high burnup, the creep rate becomes nearly infinite at a stress level equal to the yield stress. Conversely, the lower the stress relative to the yield strength, the lower the stress exponent becomes. We further know, intuitively and from the available post-irradiation thermal creep data, that prior irradiation reduces the thermal creep rate significantly. In the case of the Gras et al. model, the reduction

factor is 9 and 15 for the primary and secondary components respectively. This suggests that the reduction in the creep rate can be simulated by reformulating the creep equation in terms of the stress/yield-strength ratio, or the stress/ultimate-strength ratio in the case of strain-hardening materials, and then changing the model constants. This is illustrated by operating on the stress term in Eq. 2 as follows:

$$f_1(\sigma) = c * \sigma^n = C * (\sigma / \sigma_u)^n \tag{3}$$

where

$$C = c * \sigma_{uo}^n \tag{4}$$

In the above, c and σ_{uo} are respectively the original model constant and the test-material ultimate strength. They retain their values as originally determined for the test specimen. However, when the model is applied to irradiated material, its ultimate strength σ_u is used in the creep equation as shown by Eq. 3. Equations (3) and (4) show that the reduction in the creep rate between unirradiated and irradiated material would be of magnitude equal to r^n, where r is the ratio of their ultimate strengths. For other forms of stress dependencies, e.g., hyperbolic sine function, the procedure is a bit more complicated, but the principle is the same. It should be noted, however, that the procedure may require the use of adjustable parameters to accomplish satisfactory fit. This procedure can be validated using existing thermal creep data of irradiated materials such as the Goll et al. [61] data discussed earlier.

Remarks on Secondary Creep: The creep model expressed in Eqs. 1 and 2 implies that the model parameters can be quantified from separately developed primary and secondary creep data. Since it is difficult to separate the primary and the secondary creep boundaries in conventional constant-load creep tests, the process becomes subject to interpretation. The following remarks are given here to caution against erroneous interpretation of creep data and the impact of such interpretation on assessing the creep capacity of spent fuel cladding during long-term storage. Such erroneous interpretation has already occurred in the course of NRC's review of the Wesflex licensing submittal.

The notion that the secondary creep rate can be easily determined from standard creep tests is not borne out by experience. In a constant force (constant pressure) test, the true stress is changing, especially when the creep regime transitions from secondary to tertiary. Under high stress and high temperature the time rate of change may be high enough to cause almost immediate transition from primary to tertiary creep. Such a response is quite evident in the creep rupture test of Limon et al., Figure 4-3. The only way to observe and measure secondary creep, if it exists at all, is in a constant-stress test, which is far more difficult to perform. In fact the whole concept of designating primary, secondary and tertiary, as separate creep regimes is introduced simply for the convenience of deriving creep equations from data. Unfortunately, the process has been confused with fundamental material behavior, and analysts began to look for these regimes in the data and superimpose their own extrapolations without justification. Let us take, for example, a creep model of the Limon et al. type, which does not exhibit a secondary (constant with time) rate. To derive a constant creep rate from the model (or its data), a time window during which the creep rate is assumed to remain constant would have to be arbitrarily chosen.

Depending upon the objectives of the analyst, e.g., to demonstrate early exhaustion of creep strength, the analyst would choose an early time window, which exaggerates the secondary creep rate. Conversely, another analyst with a different objective would choose a later time window. Since secondary creep is not easily quantifiable without conducting constant-stress creep tests, the process will remain somewhat subjective and hence controversial to some extent.

Effects of In-situ Annealing and Damage Recovery

There are three sources of hardening in Zircaloy cladding that may be subject to thermal annealing during dry storage: cold work, fast fluence and hydrogen. Annealing of cold work and irradiation-induced hardening are temperature and time dependent, and the time-at-temperature becomes the governing variable in evaluating the degree of recovery for these two sources of hardening. Hydrogen-induced hardening, on the other hand, is not subject to increasing recovery with increasing hold time. Hydride-induced hardening may be enhanced during dry storage because of the drop in the hydrogen solubility due to the decreasing temperature with time, which causes the excess hydrogen to re-precipitate as zirconium hydrides, causing a slight increase in the hydrides concentration. This effect has been discussed in Section 3 of this report. With respect to the creep behavior, however, hydriding increases the cladding resistance to creep, similarly to irradiation-induced hardening, and will remain unchanged during dry storage.

As already mentioned, long-time exposure of the cladding to high temperature can cause partial annealing of cold work, and perhaps full re-crystallization if higher temperature is maintained for the appropriate length of time. This has the effect of changing the creep rate with time, initially to higher values and later to lower values at longer time, with the consequence of introducing uncertainties in the creep predictions [62]. Open literature data for cold-work stress-relieved (CWSR) material show a linear dependence in log-log scale of the beginning-of-recovery (BOR) and the end-of-recovery (EOR) temperatures in °C on hold time in hours. Bouffioux and Legras [67] conducted annealing test of CWSR Zircaloy-4 17x17 hydrided specimens over a temperature range covering 400°C to 520°C and hold time from 1 hour to 1000 hours. The hydrides in the samples, in the form of circumferentially oriented platelets, ranged from 100 ppm to 350 ppm at the test temperatures. Bouffioux and Legras found that hydriding inhibits the recovery in CWSR Zircaloy-4 by increasing the hold time, relative to the literature data, for the BOR temperature and the EOR time to achieve full re-crystallization. Creep tests of hydrided specimens (560 ppm) conducted at 400°C, which involved zero recovery, showed a creep rate reduction factor of five relative to the as-received specimens. However, creep tests of specimens with higher hydrogen content (720-760 ppm) conducted at 470°C for 250 hours showed only a factor of three reduction in the creep rate relative to the as-received specimens. This can be attributed to the partial annealing of cold work, which amounted only to 25% at 470°C.

The Bouffioux and Legras data can be used to determine the time-temperature domain to avoid during dry storage and for determining creep data. The temperature-time dependence for BOR can be approximated by $T = 508t^{-0.0301}$ from the Bouffioux and Legras data. This formula aids in estimating the length of incubation time allowed for a given temperature. For example at 450°C, the incubation time is about 56 hours, whereas at 400°C the incubation time is 2800 hours, increasing to 27 years at 350°C. This indicates that recovery consequences can be avoided by the

limiting the initial storage temperature and the vacuum drying time. Also, accelerated creep tests longer than 2800 should not be conducted at temperatures above 400°C.

Annealing of irradiation damage does not necessarily follow the same behavior as cold work annealing. For example, the effect of hold time on irradiation-damage annealing is not as strong as that for cold work. The majority of the data was generated under transient temperature conditions to study cladding behavior under LOCA, (MATPRO data base [79]). However, the data indicate that irradiation damage annealing becomes significant for temperatures above 425°C (Ref. 79, Table B-9.V).

Acceptance Criterion – Creep-Strain-Based Limit

Current State of Practice: Until the submittal of BFS's Wesflex Spent Fuel Dry Storage System (Docket Number 72-1026) to NRC for review, the state of practice has mainly remained in the technical arena, dealing with dry storage issues from two different perspectives: traditional approaches of using phenomenological creep models and strain-based criterion to determine the maximum initial storage temperature; and mechanistic failure models, namely the DCCG/CSFM methodology, which characterizes cladding failure as a void nucleation and growth mechanism. The practical difference between the two approaches is that the limit state in the latter approach is not directly measurable, whereas in the former approach cladding failure is based on measured data. In the absence of validation data, it is not possible to determine from the DCCG/CSFM approach the cladding's residual creep capacity to enable the estimation of safety margins. Besides these practical limitations, however, the applicability of the DCCG methodology to Zircaloy materials, either as the primary failure mechanism as proposed by LLNL, or as used by PNNL in a life-fraction rule within the CSFM methodology, has been called to question (see EPRI TR-103949, May 1994 [7] and UCRL-ID-131098, Dec. 1999 [6]). Void nucleation and growth is discussed in Franklin et al. ("Creep of Zirconium Alloys in Nuclear Reactors", STP 815, American Society For Testing and Materials, 1983 [62]). The authors' conclusions are that "…void nucleation and growth in zirconium alloys does not appear to be of significant technological importance for water reactor applications." EPRI studies (EPRI NP-5591, January 1988) provide additional, relevant information on the effects of irradiation temperature and neutron flux on the microstructural evolution in irradiated Zircaloys. The absence of voids in Zircaloy claddings irradiated in light water reactors leads to questioning the relevance of DCCG as a limiting governing mechanism.

The staff acceptance of a strain-based model has been exercised in the Wesflex review. The reviewers accepted the 1% strain criterion, but recommended severe restrictions on the oxide thickness [71], relying on unrealistic interpretations of material property data generated for other applications.

The proposed approach is based on the technical consensus that creep is the governing mechanism, and by adopting a quantifiable strain limit with adequate margin against failure, one can be reasonably assured of no creep rupture during storage. This strain limit criterion is presented below.

Proposed Criterion - 2% Strain Limit: Einziger et al. [78] conducted integral creep experiments in the early eighties using Westinghouse PWR rods, with burnup in the range 16-18 GWD/MtU, subjected to temperatures of 482°C to 571°C for a period of up to 7600 hours. Initial cladding stresses due to fission gas and pre-pressurization were in the range of 40 to 75 MPa. Post-test creep strains in the middle portion of the rods, where uniform creep prevailed, were in the range of 1.7% to 7%. No gross degradation of the fuel rods or cladding cracks were detected. On the basis of these tests, it is possible to conclude that at maximum temperatures less than 400°C, a total cladding strain of 2-3% has no negative effect on cladding integrity (Peehs et al. [76]).

More recent creep data (W. Goll, E. Toscano, and H. Spilker, KTG "Brennelemente und Kernbauteile, Karlsruhe, Feb 29-Mar 1, 2000 [61]) have shown that a creep strain capacity greater than 2% has been achieved in accelerated creep tests conducted at two temperatures, 300°C and 370°C, for stress levels ranging from 320 to 630 MPa. The failure strains in these tests were in the range of $\geq$ 2.5% to $\cong$ 6%. Although the stresses were necessarily raised well above dry storage conditions to achieve large creep strain within short time, the temperatures are in the proper range and below the damage recovery boundary [67]. Therefore, the Goll et al. data is extrapolatable in the stress-strain space to lower stresses typical of storage conditions. Creep rupture data by Bouffioux and Rupa [68] showed creep ductility of 9-12% at 350-400°C and 350-386 MPa for hydrided samples with hydrogen content in the range 215-1040 ppm. What is most interesting about these tests is that the hydrided samples showed similar ductility to the as-received samples, but the failure time was 2-6 times greater. Although the samples came from unirradiated 17 x 17 tubing, hydrogen hardening exhibited similar effect to irradiation hardening. We conclude from the above that a 2% strain criterion is supported by current data.

The proposed criterion has sufficient margin against rupture, at least within the 0.5% failure probability stated in the SRP. The strain limit of 2% can be shown to be an asymptotic limit, which implies that cladding integrity will be assured even after the lapse of the licensed storage time. This will be demonstrated through creep analysis planned in the coming year using EPRI's ESCORE/FREY/FALCON family of fuel behavior codes. In the mean time, however, for the purpose of this report, we can show by simple hand calculations that creep deformations of a closed constant-mass system are self-limiting because of the feedback between the cladding deformations, the gas pressure and the continuously decreasing temperature. The initial void volume of a typical fuel rod is typically 25 cm^3, or less, of which roughly 70%, or 17.5 cm^3, is in the plenum. For the purpose of calculating the effect of gas volume change on the gas pressure, one can conservatively assume that the fuel stack free volume remains unchanged. A creep strain of 1% is equivalent to an increase in the fuel rod void volume of about 5 cm^3. The effect of this increase in the void volume on the fuel rod pressure, assuming continuous communication with the plenum, is 5/(5+25) or about 17%. This results in a 17% reduction in the cladding stress, but a 43% reduction in the creep rate, assuming a power law or a hyperbolic sine law. This reduction in creep rate grows to 64% at a creep strain of 2%. In addition, the decreasing temperature has a far stronger effect. A 50°C decrease in temperature reduces the creep rate by a factor of 100. Spilker et al. [69] have shown similar trend to support CASTOR V initial storage temperature limits.

Effects of Oxide Spallation on the Proposed Criterion: Oxide spallation can lead to the formation of highly brittle hydride lenses penetrating a distance of one-third to one-half of the cladding

thickness. However, the cladding ligament beneath the hydride lens remains fairly ductile, with local plastic strain several times greater than the rest of the cross section because of strain localization effects. The burst plastic-strain value of 0.58% reported by Garde et al. [55] for cladding with spalled oxide represents averaged value over the cross-section, which translates into localized strain value in the remaining ligament of the order of 3-4%, depending upon the circumferencial extent of the hydride lens. In fact, Garde et al measured the local plastic strain in the ligament beneath the hydride lens to be slightly above 3% (see Figure 4-2 of Garde's paper). When the corresponding elastic strains to the average and the local strains are added, the total strains become 1.1% and 4% respectively. Had the same tube specimen been subjected to a creep test, the average and the local creep strains at the time of failure would certainly be higher because of strain rate effects, Fuketa et al [66]. We will attempt to derive an analytical creep-rupture simulation of the Garde et al burst test, from which we can derive a criterion for cladding with spalled oxide. This is discussed below.

It can be shown that strain localization is a strong function of the stress exponent in the stress-strain relation governing plastic deformations. In the high strain-rate regime of tensile and burst tests, the stress exponent can exceed 10; whereas in the low-stress, low strain-rate creep regimes, the stress exponent is in the range of 2-3. Thus, creep-strain localization in the ligament under the hydride lens does not rise to the same intensity as strain localization in the high strain-rate tensile or burst tests. We consider two strain-stress relations, one that governs the fast-pressurization burst test of the Garde et al. variety, and one that applies to a constant-pressure creep test. It can be shown that both of these relations reduce to the form $\varepsilon = A\sigma^n$, but with different values for A and n. This form allows derivation of a strain localization factor for a cladding with local thinned region.

In the case of high strain rate tests, the stress-strain state in the plastic regime is governed by an equation of the following type (MATPRO database [79]).

$$\sigma = K\varepsilon^S\left(\frac{\dot{\varepsilon}}{\dot{\varepsilon}_0}\right)^m \tag{5}$$

We invert this formula to obtain

$$\varepsilon = \left(\frac{\dot{\varepsilon}}{\dot{\varepsilon}_0}\right)^{-mn} K^{-n}\sigma^n,\ n = 1/s \tag{6}$$

In Eq. 6, K, s and m are, respectively, the strength coefficient, the hardening coefficient and the strain-rate sensitivity coefficient. For irradiated Zircaloy in the temperature range of interest, MATPRO gives m = 0.02, s = 0.1, n = 10, and $\dot{\varepsilon}_0 = 10^{-3}$/s for the reference strain rate. For a constant strain rate test, Eq. 6 has the following power law:

$$\varepsilon = A\sigma^n \tag{7}$$

In the case of low strain rate tests, a steady-state creep law of the type shown in Eq. 2 applies, in which the stress dependence is either a hyperbolic sine function or a power law with exponent n.

For the stress range of interest, the hyperbolic sine function is equivalent to a power law with n = 3. Such a creep law has the same stress dependency as represented by Eq. 7.

Now we consider a test specimen in which the cladding exhibits the same physical condition as in the Garde et al. test. For the type of stress-plastic-strain relation described by Eq. 7, it is easy to show, from equilibrium considerations, that the following relationship holds for the average hoop strain and the local hoop strain in a tube with localized thinning,

$$\varepsilon_a = \varepsilon_\ell \left[\frac{\theta}{2\pi} \left(1 - \alpha^n\right) + \alpha^n \right] \tag{8}$$

where ε_a and ε_ℓ are the average and local strains respectively, α is the ligament/thickness ratio, and θ is the subtended angle in radians of the thinned section, which includes the hydride lens and the peripheral damage areas. The inverse of the quantity in the square brackets is the concentration factor which, for a large n, as in the case of Garde's fast pressurization test, reduces to the quantity $2\pi / \theta$. As θ shrinks to zero, i.e., approaching the geometry of a sharp crack, the concentration factor approaches infinity, and the behavior of the specimen is governed by fracture mechanics. Conversely, the concentration factor approaches unity for the case of uniform thickness reduction, and therefore no strain localization is possible. In order to estimate the magnitude of the average hoop strain ε_a, we need estimates for ε_ℓ and θ. The angle θ is estimated from micrographs in Garde et al. [55] and Smith et al. [59] to be approximately $\pi / 3$. We assume a 50% wall thinning, which gives an α value of 0.6 of the wall thickness remaining after subtracting the thickness loss due to corrosion. Substituting the following values, $\theta = \pi / 3$, $\alpha = 0.6$, n = 10, and $\varepsilon_\ell = 0.03$ for the local plastic strain as measured by Garde et al. in Eq. 8 gives an average plastic strain $\varepsilon_a = 0.52\%$, which agrees well with the measured value of 0.58%. This is considered to be a validation of the method, which is now applied to the creep-rupture simulation as shown below.

First, a highly conservative assumption is made: the local creep ductility in the creep specimen is equal to the total strain capacity, i.e., elastic + plastic, of the Garde et al. specimen, ignoring strain-rate effects. The local elastic strain is simply the local stress, which is roughly 1.7 times the average hoop stress, divided by the elastic modulus. Thus the total strain in the Garde specimen is approximately 4%. Note that the elastic strain at dry-storage stress at the time of assumed rupture would be less than 0.1%. Using Eq. 8 with the same values of α and θ, but with n = 3, which is valid for creep, we obtain ε_a = 1.4%. Adding the elastic component to this value gives a circumferentially averaged strain of 1.5%. This strain is the lower-bound value that would be measured in a constant-pressure/constant-temperature creep specimen of physical condition similar to the Garde et al fast pressurization test of spalled cladding. Next, strain rate effects are considered.

Fuketa et al. [66] showed a difference of a factor of 2 between the average residual strains measured in pressurized hydrided cladding samples tested at two strain rates three orders of magnitude apart (see Fig. 19 of the cited paper). Creep strain rates for dry-storage stresses and temperatures differ by 6 orders of magnitude from fast pressurization tests conducted by Fuketa et al. and Garde et al. Fuketa's results indicate that if the Garde's test were to be conducted at a pressurization rate 10^{-3} lower, the specimen strains would be: ε_a = 1.16% plastic and ε_ℓ = 7%

(6% plastic + 1% elastic). With ε_ℓ = 0.07 as the equivalent creep ductility, Eq. 8 gives an average creep strain value of 2.4%, or a total (elastic + plastic) strain of 2.5%.

Considering the fact that we have used conservative values in the above calculations, a strain value of 2% can be justified. For fuel rods with suspected spallation that have been normally discharged from reactors, there still exists a greater margin in the cladding strain capacity than indicated by either of the 1.5% or the 2.5% values calculated for severely spalled cladding. This margin can be demonstrated by applying the Garde et al. data to creep rupture, not directly as shown above, but with the aid of a transfer function using an energy-based failure model, namely, the Critical Strain Energy Density (CSED) [56,57]. The minimum Critical Strain Energy Density (CSED), which is the mechanical energy used to fail the material, is calculated for the Garde data with spalled oxide to be 4 MPa (see Figure 3-4). The following relationship between the quantities CSED and K_{IC}, i.e. $K_{IC} = 3.5\sqrt{CSED}$ [58], was presented earlier in Section 3 of this report. Using this relationship, a fracture toughness value of 7 MPa$\sqrt{m}$ for a cladding with spalled oxide and hydride lens of thickness equivalent to half the cladding wall is obtained. Now, let us consider the spalled-rod situation under creep. With a hoop stress of 120 MPa and a total strain of 1.5%, we calculate a Strain Energy Density (SED) of 1.68 MPa. This gives a stress intensity factor K_I of 4.5 MPa$\sqrt{m}$ compared to a K_{IC} value of 7 MPa$\sqrt{m}$, which indicates a safety factor of 1.5 against mechanical fracture after a strain of 1.5 % under creep during dry storage. For the 2.5% case, the corresponding safety factor becomes 1.14. The SED estimates, and consequently the safety factors, are conservatively calculated because the stress of 120 MPa is assumed to remain constant with time.

In summary, two limits have been derived for spalled cladding. The first is a lower bound limit of 1.5% based on the highly conservative assumption that the cladding strain capacity under creep remains the same as in fast pressurization test, which most observers would consider unrealistic. By relaxing this assumption somewhat, a second limit of 2.5% was derived using the same analytical simulation. Thus, the 2% criterion remains valid, as proposed, for all cladding types without special consideration given to oxide thickness or spallation condition.

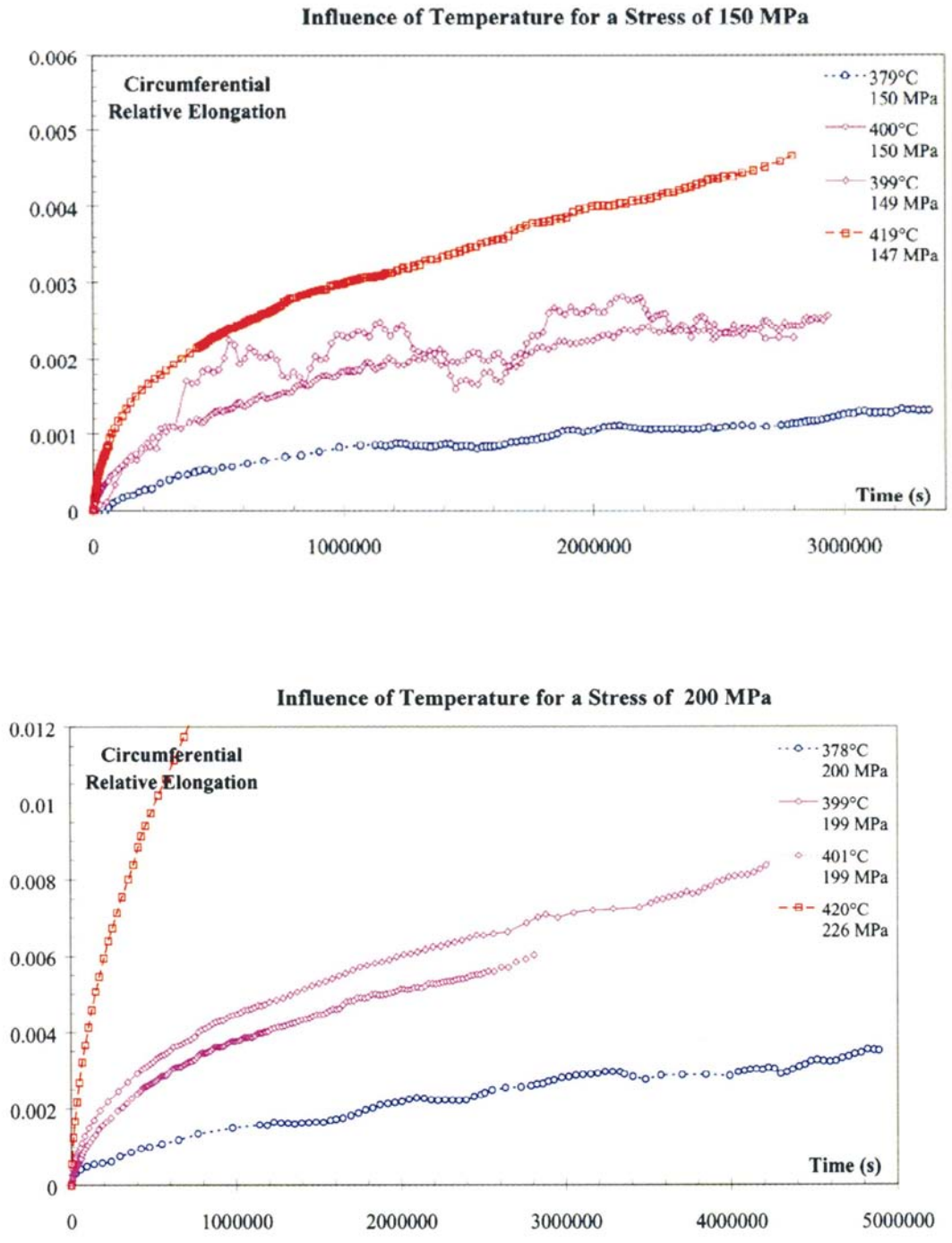

Figure 4-1. Creep of Irradiated CWSR Zircaloy-4 at Various Temperatures and Stresses (Ref. 63)

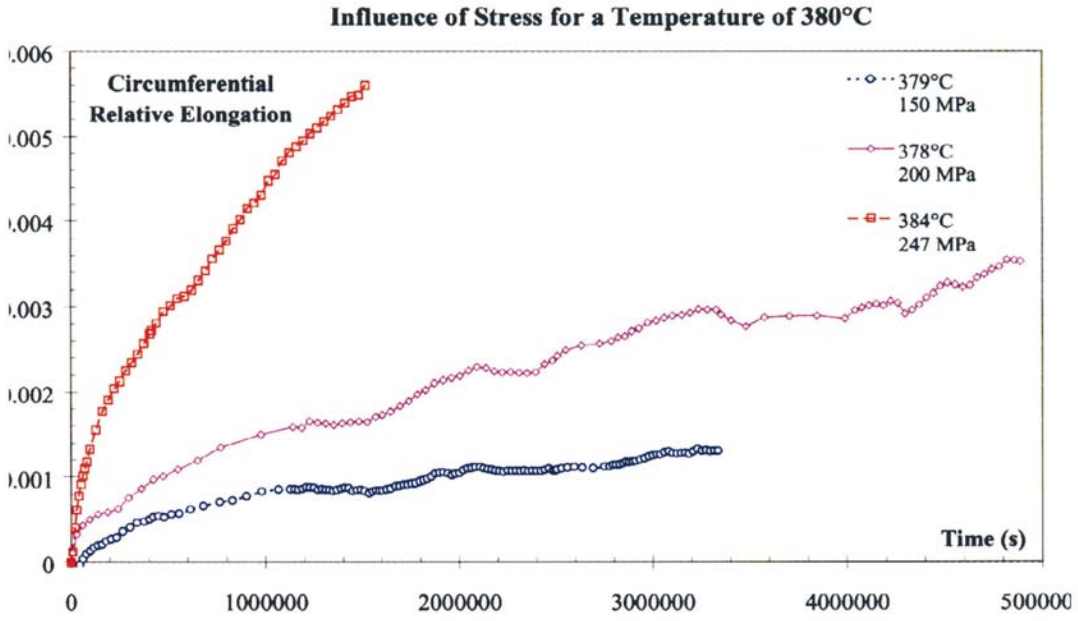

Figure 4-2. Creep of Irradiated CWSR Zircaloy-4 (Ref. 63)

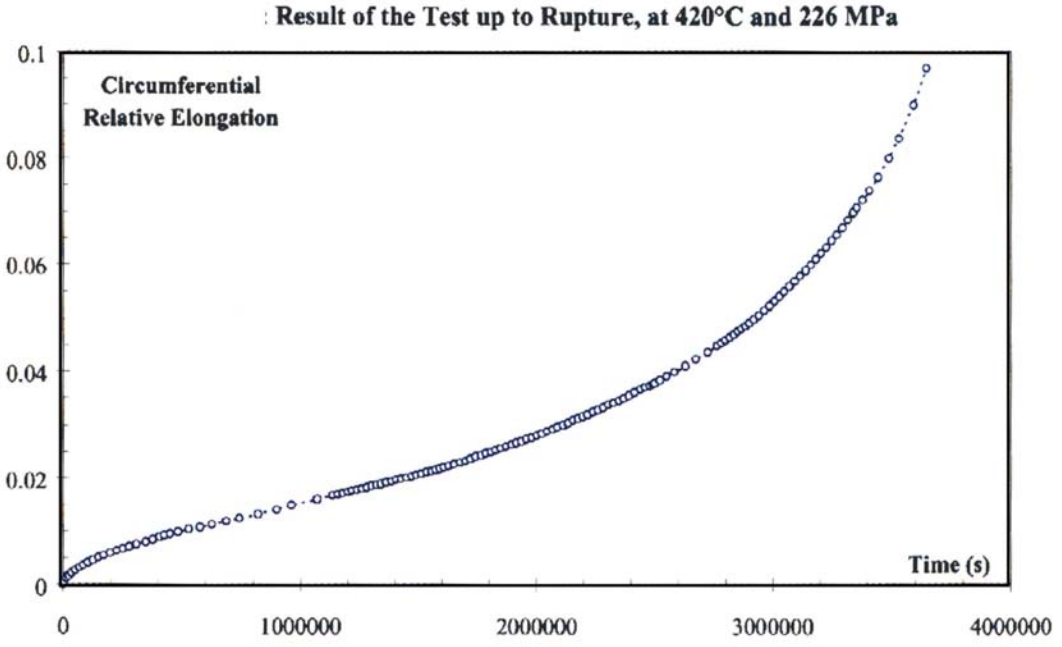

Figure 4-3. Creep Rupture Curve for Irradiated CWSR Zircaloy-4 Showing Primary-to-Tertiary Transition (Ref. 63)

5

PIN-HOLE-EQUIVALENT FAILURE MODE

At high burnup, the fuel pellets are virtually bonded to the cladding, and the gas pressure in the free volume within the fuel stack is transmitted to the cladding indirectly through interlocked fuel fragments. This constrains the cladding from freely deforming as an empty tube and prevents the development of balloon-type deformations with the potential for relatively large rupture openings. Consequently, the failure mode in high burnup cladding tends to be in the form of a narrow axial crack. Thus, the reduced ductility of high burnup cladding, ironically, has the beneficial effect of limiting the width of the failure opening. Burst tests by Fuketa et al. (Park City ANS Topical Meeting, April, 2000 [66]) show that hydrided cladding burst-tested at room temperature exhibited narrow axial cracks compared to more ductile specimens that showed typical burst opening.

In order to demonstrate that the size of the failure opening is equivalent to a pin-hole, we apply the leak-before-break criterion proposed by Irwin et al. [70]. Irwin was the first to relate material toughness to the mode of failure in a pressurized structure. The leak-before-break criterion provides the means of estimating the necessary toughness of pressure-vessel steels so that a thumb-nail crack would grow through the wall in a self-similar manner, and could be detected before the leak can progress to a burst. The uncertainty in this theoretical analysis is a function of the radius to thickness ratio, the closer this ratio to a thick-wall vessel, the lower the uncertainty of the predictions. It is interesting to note that the fuel rod is comparatively a much thicker pressure vessel than the reactor vessel.

The thumb-nail crack geometry for the leak-before-burst criterion is a crack surface in the shape of a parabola, with a length (at the inner surface) of twice the cladding thickness, and a depth equal to the cladding thickness, i.e., the crack just touches the outer surface. The stress intensity K_I for such a crack under a low stress compared to the material's yield strength is given by

$$K_I^2 = 1.12\,\pi\,\sigma^2\,a \qquad (9)$$

At fracture $K_I = K_C$, where K_C is the plane-stress fracture toughness, which applies to cladding geometry. We make use of the plane-strain $K_{IC} = 7.8$ MPa $\sqrt{m}$, which was estimated from Garde's et al. data in Section 3 for cladding with oxide thickness greater than 100 μm. The K_C value that corresponds to K_{IC} is larger, but the difference can be ignored here for conservatism. We can now calculate the maximum value of the stress that should not be exceeded if burst failure is to be avoided. Using a = 600 μm, $K_I = K_{IC} = 7.8$ MPa $\sqrt{m}$, Eq. 9 yields $\sigma = 170$ MPa. As can be seen, this value is higher than the maximum stress in the cladding, which is assumed to exist at the beginning of dry-storage life. This demonstrates that in the event of fracture, the crack will propagate slowly in a self-similar manner until it penetrates the wall and depressurizes

the rod before it can extend axially in a burst mode. The above calculations are valid for all cladding conditions regardless of oxide thickness or the state of the oxide, coherent or spalled.

6

SUMMARY AND CONCLUSIONS

Studies presented in this report confirm the general technical consensus that creep is the governing mechanism for spent fuel in long-term dry storage. Postulated failure mechanisms, namely, stress corrosion cracking (SCC), delayed hydride cracking (DHC) and creep rupture (CR), have been examined in detail from two perspectives: the initial environments in which they were developed and applied, and their applicability to dry storage conditions. With respect to the former, this report serves as a state of the art review, and with respect to the latter, the report presents cogent arguments in favor of, or against, extending the operative range of each of the postulated mechanisms to spent fuel dry storage. In doing so, reliance is made on well-founded extrapolation techniques to transfer the mechanisms from their initial in-reactor and laboratory domains to out-of-reactor spent fuel dry storage environments. This transfer has been done both qualitatively where necessary and quantitatively when possible, with fracture toughness used as the quantitative transfer function. In this regard, the report provides useful information on cladding fracture toughness estimates, recognizing the specific physical conditions of the cladding, which may not be found elsewhere in the literature. The report findings are summarized below.

(1) The chemical environment that promotes in-reactor SCC, (PCI failures), is sub-critical to be operative in dry storage.

(2) Under the most restrictive conditions, the cladding stress during dry storage remains below the SCC threshold stress.

(3) High-burnup effects are insufficient factors for increasing SCC susceptibility during dry storage.

(4) There may be troublesome aspects of the cladding thermal history with respect to DHC and re-crystallization, which can be avoided by limiting high temperature excursions and cycling during vacuum drying. Other factors, however, come into play (see (5) below).

(5) The continuously decreasing cladding temperature with time, especially if the initial drying temperature excursions are sufficiently high, can potentially promote DHC. However, the cladding stress intensity K_I for conservatively estimated incipient cracks remains below the fracture toughness K_{IH} for Stage-I DHC initiation.

(6) Although post-irradiation thermal creep data is not robust, there is sufficient information to perform modeling and analysis to reach valid conclusions. Future data, however, would be appropriate to confirm properly posed creep analyses that can be performed at present.

(7) Careful interpretation of the creep data generated in conventional constant-load creep tests is needed before it can be extrapolated to long-term creep behavior.

(8) Creep rupture can be avoided by limiting the creep strain to an appropriately low value (see (9) below).

(9) An acceptance criterion of 2% creep strain, supported by existing data, is proposed. This value is appropriately characterized as an asymptotic limit, which can be demonstrated analytically, and is easy to confirm experimentally. This strain limit is shown to be valid for fuel conforming to approved zirconium oxide limits, including fuel characterized by the presence of hydride lenses on the outer surface of the cladding.

(10) Using a classical leak-before-break analysis technique, the failure mode is shown to be equivalent to a pin hole.

7

REFERENCES

1. U. S. Nuclear Regulatory Commission, "Standard Review Plan for Dry Cask Storage System: Final Report," NUREG-1536, January 1997.

2. U. S. Nuclear Regulatory Commission (NRC), "Safety Evaluation Report Related to the Topical Safety Analysis Report for CASTOR V/21 Dry Spent Fuel Storage Cask - Appendix A: Analysis of Diffusion Controlled Cavity Growth (DCCG) Damage to Fuel Cladding in Dry Storage," September 1985.

3. Schwartz, M. W. and Witte, M. C., "Spent Fuel Cladding Integrity During Dry Storage," Lawrence Livermore National Laboratory, UCId-21181, September 1987.

4. Raj, R. and Ashby, M F., "Intergranular Fracture at Elevated Temperature," Acta Met., V23, pp. 653-666, 1975.

5. Chin, B. A., Khan, M. A., Tam, J. C. L., and Gilbert, E. R., "Deformation and Fracture Map Methodology for Predicting Cladding Behavior During Dry Storage," Pacific Northwest Laboratory, PNL-5998, 1986.

6. Hayes, T. A., Rosen, R. S., and Kassner, M. E., "Critical Analysis of Dry Storage Temperature Limits for Zircaloy-Clad Spent Nuclear Fuel Based on Diffusion Controlled Cavity Growth," December 1999.

7. Pesatore, C. and Cowgill, M., "Temperature Limit Determination for the Inert Dry Storage of Spent Nuclear Fuel," EPRI TR-103949, Project 3290-03, May 1994.

8. U. S. Nuclear Regulatory Commission, Spent Fuel Project Office Interim Staff Guidance - 11, May 13, 1999.

9. Rosenbaum, H. S., *Electrochemical Technology*, Vol. 4 1966, p. 153.

10. Garlick, A. and Wolfenden, P. D., *Journal of Nuclear Materials*, Vol. 41, 1971, p. 274.

11. Wood, J. C., *Journal of Nuclear Materials*, Vol. 45, 1972/73, p. 105.

12. Wood, J. C., *Nuclear Technology*, Vol. 23, 1974, p. 63.

13. Busby, C. C., Tucker, R. P., and McCauley, J. E., *Journal of Nuclear Materials*, Vol. 55, 1975, p. 1.

14. Cox, B. and Wood, J. C., *Corrosion Problems in Energy Conversion and Generation*, C.S. Tedman Jr., Ed., Pub. The Electrochemical Society, P. 275-321, 1974.

15. Cox, B., "Reviews on Coatings and Corrosion," Vol. 1, No. 4, 1975, Freund, Tel Aviv, p. 366.

16. Coleman, C. E. and Ambler, J. F. R., "Zirconium in the Nuclear Industry," ASTM STP 633, p. 589.

17. Wood, J. C., Surette, B. A., London, I. M., and Baird, J., *Journal of Nuclear Materials*, Vol. 57, 1975, pp. 155.

18. Roberts, J. T. A., Jones, R. L., Cubicciotti, D., Miller, A. K., Wachob, H. F., Smith, E., and Yaggee, F. L., "A Stress Corrosion Cracking Model for Pellet-Cladding Interaction Failures in Light-Water Reactor Fuel Rods," Zirconium in the Nuclear Industry (fourth Conference), ASTM STP 681, American Society for Testing and Materials, 1979, pp. 285-305.

19. Miller, A., Challenger, D., and Tasooji, A., "SCCIG-A: Phenomenological Model for I-SCC of Zry," EPRI Report NP 1978, Electric Power Research Institute, Palo Alto, CA.

20. Rosenbaum, H. S., Rand, R. A., Tucker, R. P., Cheng, B., Adamson, R. B., Davies, J. H., Armijo, J. S., and Wisner, S. B, "Zirconium-Barrier Cladding Attributes," Zirconium in the Nuclear Industry: Seventh International Symposium, STM STP 939, American Society for Testing and Materials, Philadelphia, 1987, pp. 675-699.

21. Rashid, Y. R., "Mathematical Modeling and Analysis of Fuel Rods," *Nuclear Engineering and Design*, Vol. 29, 1974, pp.23-33.

22. Brunisholz, L. and Lemaignan, C., "Iodine-Induced Stress Corrosion of Zircaloy Fuel Cladding: Initiation and Growth," Zirconium in the Nuclear Industry: Seventh International Symposium, ASTM STP 939, American Society for Testing and Materials, Philadelphia, 1987, pp. 700-716.

23. Rashid, Y. R. and Nerman, H., "Application of SAFE-2D Program to the Analysis of Fuel-Rod Ramp Tests," International Conference on World Nuclear Energy, ANS 1976 Winter Meeting, Nov. 14-19, p. 170.

24. Davies, J. H., Rosenbaum, H. S., Armijo, J. S., Proebstle, R. A., Rowland, T. C., Thompson, J. R., Esch, E. L., Romeo, G., and Rutkin, D. R., "Irradiation Tests to Characterize the PCI Failure Mechanism", ANS Topical Meeting on Water Reactor Fuel Performance, St. Charles, Illinois, 1977, pp. 230-242..

25. Hollowell, T. E., Knudsen, P., and Mogard, H., "Proceedings ANS Topical Meeting on LWR Extended Burnups - Fuel Performance and Utilization," Williamsburg, VA, USA, April 1982, Vol. 1, p. 4-5.

26. Knaab, H., Lang, P. M., and Mogard, H., "Proceedings IAES Specialists' Meeting on Power Ramping and Cycling Behavior of Water Reactor Fuel," Petten, September 1982.

27. Mogard, H. and Heckermann, H., "Proceedings ANS Topical Meeting on Light-Water Reactor Fuel Performance," Orlando FL, USA, April 1985, Vol. 2, p. 6-17.

28. Mogard, H., Knaab, H., Bergenlid, U., and Lysell, G., *Nucl. Technol*, 69 (1985) 236.

29. Davies, J. H., Rosicky, E., Esch, E. L., and Rowland, T. C., "Fuel Ramp Tests in Support of a Barrier Fuel Demonstration," GEAP-22076, July 1984.

30. Rosenbaum, H. S., Davies, J. H., Adamson, R. B., Armijo, J. S., Rosicky, E., Wisner, S. B., Tucker, R. P., and Esch, E. L., "Resistance of Zirconium Barrier Fuel to Pellet-Cladding Interaction," Transactions of the American Nuclear Society, Vol. 38, 1981, pp. 270-272.

31. Rosenbaum, J. S., Davies, J. H., Adamson, R. B., Tucker, R. P., Rowland, T. C., Paustian, H. H., and O'Boyle, D. R., "Large Scale Demonstration of Barrier Fuel," in Proceedings, ANS Topical Meeting on LWR Fuel Performance, American Nuclear Society, Orlando, Fla., April 1985, pp. 7-63 - 7-78.

32. Busby, C. C., Tucker, R. P., and McCauley, J. E., *Journal of Nuclear Materials*, Vol. 55, 1975, pp. 64-82.

33. Peehs, M., Stehle, H., and Steinberg, E., "Out-of-Pile Testing of Iodine Stress Corrosion Cracking in Zircaloy Tubing in Relation to the Pellet-Cladding Interaction Phenomenon," Zirconium in the Nuclear Industry (Fourth Conference), ASTM STP 681, American Society for Testing and Materials, 1979, pp. 244-260.

34. Cubicciotti, D. and Davies, J. H., *Nuclear Science and Engineering*, Vol. 60, 1976, p. 314.

35. Tasooji, A., Einziger, R. E., and Miller A. K., "Modeling of Zircaloy Stress-Corrosion Cracking: Texture Effects and Dry Storage Spent Fuel Behavior", Zirconium in the Nuclear Industry: Sixth International symposium, ASTM STP 824, American Society for Testing and Materials, 1984, pp. 595-626.

36. Cox, B. and Haddad, R., "Recent Studies of Crack Initiation During Stress Corrosion Cracking of Zirconium Alloys", Zirconium in the Nuclear industry: Seventh International Symposium, ASMT STP 939, American Society for Testing Materials, Philadelphia, 1987, pp. 717-733.

37. Syrett, B. C., Cubicciotti, D., and Jones, R. L., " Embrittlement of Zircaloy-4 by Liquid Cesium at 300 °C", ASTM STP 633, 1977.

38. Videm, K. and Lunde, L., " Stress corrosion Crack Initiation and Growth and Formation of Pellet-Clad Interaction Defects", ASTM STP 681, 1979.

39. Cubicciotti, D. and Jones, R. C., "EPRI-NSA Cooperative Project on Stress Corrosion Cracking of Zircaloy," EPRI NP-717, March 1978.

40. Sejnoha, R. and Wood, J. C., "Iodine-Induced Stress Corrosion Cracking of Fixed Deflection Stressed Slotted Rings of Zircaloy Fuel Cladding." Zirconium in the Nuclear Industry (Fourth Conference), ASTM STP 681, American Society for Testing and Materials, 1979, pp. 261-284.

41. Cox, B., "Hydride Cracks as Initiators for Stress Corrosion Cracking of Zircaloys," Zirconium in the Nuclear Industry (Fourth Conference), ASTM STP 681, American Society for Testing and Materials, 1979, pp. 306-321.

42. Wood, J. C., Surrette, B., London, I., and Baird, J., *Journal of Nuclear Materials*, Vol. 57, 1975, pp. 155-179.

43. Jones, R., et al., *Journal of Nuclear Materials*, Vol. 82, 1979, pp. 26-38.

44. Videm, K., et al., *Journal of Nuclear Materials*, Vol. 87, 1979, pp. 259-267.

45. Simpson, C. J. and Ells, C. E., *Journal of Nuclear Materials*, Vol. 52, 1974, pp. 289-295.

46. Ross-Ross, P. A., Adams, E. J., Dixon, D. F., and Metcalfe, R. in "Nuclear Energy Maturity," Proceedings of the European Nuclear Conference, Paris, 1975, Pergamon Press, Oxford, 1976, pp. 85-109.

47. Dutton, R. and Puls, M. P., *Effect of Hydrogen on the Behavior of Materials*, (A. W. Thompson and I. M. Bernstein, eds) p. 516, Metallurgical Society, AIME, New York, (1976).

48. Coleman, C. E. and Ambler, J. F. R., "Susceptibility of Zirconium Alloys to Delayed Hydrogen Cracking," *Zirconium in the Nuclear Industry*, ASTM-STP 633, 1977, pp. 589-607.

49. Simpson, L. A. and Nuttall, Keith, "Factors Controlling Hydrogen Assisted Subcritical Crack Growth in Zr-2.5Nb Alloys," *Zirconium in the Nuclear Industry*, ASTM-STP 633, 1977, pp. 608-629.

50. Simpson, L. A. and Puls, M. P., "The Effects of Stress, Temperature and Hydrogen Content on Hydride-Induced Crack Growth in Zr-2.5 Pct Nb," *Metallurgical Transactions*, Vol. 10A, August 1979, pp. 1093-1105.

51. Huang, F. H. and Mills, W. J., Delayed Hydride Cracking Behavior for Zircaloy-2 Tubing," Metallurgical Trans. A, 22A, P. 2049, 1991.

52. Efsing, P. and Petterson, K., "The Influence of Temperature and Yield Strength on Delayed Hydride Cracking in Hydrided Zircaloy 2," Zirconium in the Nuclear Industry: Eleventh

International Symposium, ASTM STP 1295, American Society for Testing and Materials, 1996, pp.394-404.

53. Montgomery, R. O. and Rashid, Y. R., "Operational Recommendations for Failed Fuel-An EPRI Perspective," ANATECH Corp., EPRI TR-107217, 3564-03, November 1996.

54. Kreyns, P. H., Bourgeois, W. F., White, C. J., Charpentier, P. L., Kammenzind, B. F., and Franklin, D. G., "Embrittlement of Reactor Core Materials," Zirconium in the Nuclear Industry: Eleventh International Symposium, ASTM STP 1295, American Society for Testing and Materials, 1996, pp.758-782.

55. Garde, A. M., Smith, G. P., and Pirek, R. C., "Effects of Hydride Precipitate Localization and Neutron Fluence on the Ductility of Irradiates Zircaloy-4," Zirconium in the Nuclear Industry: Eleventh International Symposium, ASTM STP 1295, American Society for Testing and Materials, 1996, pp. 407-430.

56. Montgomery, R. O. and Rashid, Y. R., "Evaluation of Irradiated Fuel During RIA Simulation Tests," ANATECH Corp., EPRI TR-106387, 2905-96, August 1996.

57. Rashid, Y., R., Montgomery, R. O., Lyon, W., and Yang, R. L., "A Cladding Failure Model for Fuel Rods Subjected to Operational and Accident Transients," IAEA Specialists Meeting on Fuel Modeling, Windermere, U. K., June, 2000.

58. Rashid, Y. R., "Fracture Toughness Data for Zirconium Alloys And Its Application to Spent Fuel Cladding in Dry Storage," EPRI TR-….., 2000.

59. Smith Jr., G. P., Pirek, R. C., and Griffiths M., "Hot Cell Examination of Extended Burnup Fuel From Calvert Cliffs -1, Vol. 2," EPRI TR-103302-V2, Project 2905-02, July 1994.

60. Simpson, C. J., Kupcis, O. A., and Leemans, D. V., "Hydride Reorientation and Fracture in Zirconium Alloys," Zirconium in the Nuclear Industry, ASTM STP 633, American Society for Testing and Materials, 1977, pp. 630-642.

61. Goll, W., Spilker, H., and Toscano, E., "Short-Time Creep and Rupture Tests on High Burnup Fuel Rod Cladding," Paper submitted to JNM, May, 2000.

62. Franklin, D. G., Lucas G. E., Bement, A. L., "Creep of Zirconium Alloys in Nuclear Reactors," ASTM STP 815, 1985.

63. Limon, R., Cappelaere, Ch., Bredel, Th., Bouffioux, P., "A Formulation of the Spent Fuel Cladding Creep Behavior for Long Term Storage," LWR Fuel Performance Meeting, Park City, Utah, April 10-13, 2000.

64. Gras, J. M., "Entreposage Des Combustibles Usés," BILAN DU PPRD T4-97-07, EDF, Janvier 2000.

65. Wang, W.J.S. "Precipitate Stability in Zircaloy-4," EPRI NP-5591, January 1988.

66. Fuketa et al., "Behavior of PWR and BWR Fuels During Reactivity Initiated Accident Conditions," LWR Fuel Performance Meeting, Park City, Utah, April 10-13, 2000.

67. Bouffioux, P. and Legras, L. "Effects of Hydriding on the Residual Cold Work Recovery and Creep of Zircaloy-4 Cladding Tubes," LWR Fuel Performance Meeting, Park City, Utah, April 10-13, 2000.

68. Bouffioux, P. and Rupa, N., "Impact of Hydrogen on Plasticity and Creep of Unirradiated Zircaloy-4 Cladding Tubes," ASTM STP 1354, 2000.

69. Spilker, et al., *J. of N. Mat*. 250 (1997) 63-74

70. Irwin, G. R., Krafft, J. M., Paris, P. C., and Wells, A. A., "Basic Aspects of Crack Growth and Fracture," NRL Report 6598, Washington D. C., Nov. 21, 1967.

71. Gilbert, E. R., Beyer, C. E., and Simonen E. P., "Technical Evaluation Report of WCAP-15168, Dry Storage of High Burnup Spent Nuclear Fuel," February 2000.

72. Wisner, S. B. and Adamson, R. B. "Combined Effects of Radiation Damage and Hydrides on the Ductility of Zircaloy-2," *Nuclear Engineering and Design* 185, 1998, 33-49.

73. Jahreiff, J., Manzel, R., and Ortleib, E., "Influence of Hydrogen Content and Irradiation on the Mechanical Behavior of Fuel Assembly Structural Members Made of Zircaloy," Annual Nuclear Engineering Convention, Cologne, Germany, pp. 303-306.

74. Kasper, G., Peehs, M., and Steinberg, E., "Experimental Investigation of Post-Pile Creep of Zircaloy Cladding Tubes," SMIRT Conference 1985, Brussels, Paper C1/8.

75. Peehs, M., Kasper, G., and Steinberg, E., "Experimentally-Based Spent Fuel Dry Storage Performance Criteria," Proc. 3rd. Int. Conf. On Spent Fuel Storage Technology, Seattle 1986, p. S-316.

76. Peehs, M., Garzarolli, F., and Goll, W., "Assessment of Dry Storage Performance of Spent LWR Fuel Assemblies with Increasing Burnup" IAEA-SM-352-39.

,

77. Hardie, D., Shanahan, M. W., "Stress Reorientation of Hydrides in Zr2.5%Nb," *J. of Nucl. Mat*., 55, (1975) 1-13.

78. Einziger, R. E., Atkin, S. D., Stellprecht, D. E., and Pasupathi, V., "High Temperature Postirradiation Materials Performance of Spent Pressurized Water Reactor Fuel Rods under Dry Storage Conditions," *Nuclear Technology*, Vol.57, Apr. 1982, p. 65.

79. "MATPRO-Version 11 (Rev. 2) A Handbook of Materials Properties for Use in the Analysis of Light Water Reactor Fuel Rod Behavior," EG&G Idaho, Inc., Department of Energy, NUREG/CR-0497, TREE-1280, Rev. 2, August 1981.

About EPRI

EPRI creates science and technology solutions for the global energy and energy services industry. U.S. electric utilities established the Electric Power Research Institute in 1973 as a nonprofit research consortium for the benefit of utility members, their customers, and society. Now known simply as EPRI, the company provides a wide range of innovative products and services to more than 1000 energy-related organizations in 40 countries. EPRI's multidisciplinary team of scientists and engineers draws on a worldwide network of technical and business expertise to help solve today's toughest energy and environmental problems.

EPRI. Electrify the World

1001207

Printed on recycled paper in the United States of America

EPRI • 3412 Hillview Avenue, Palo Alto, California 94304 • PO Box 10412, Palo Alto, California 94303 • USA
800.313.3774 • 650.855.2121 • askepri@epri.com • www.epri.com